

DEPOSITIONAL ENVIRONMENT OF THE MIDDLE PENNSYLVANIAN GRANITE WASH;
LAMBERT 1, HRYHOR, AND SUNDANCE FIELDS, NORTHERN PALO DURO BASIN,
OLDHAM COUNTY, TEXAS

A Thesis

by

AMY LAURA WHARTON

Submitted to the Graduate College of
Texas A&M University
in partial fulfillment of the requirement for the degree of
MASTER OF SCIENCE

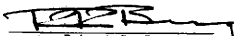
August 1986


Major Subject: Geology


DEPOSITIONAL ENVIRONMENT OF THE MIDDLE PENNSYLVANIAN GRANITE WASH;
LAMBERT 1, HRYHOR, AND SUNDANCE FIELDS, NORTHERN PALO DURO BASIN,
OLDHAM COUNTY, TEXAS

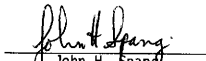
A Thesis
by
AMY LAURA WHARTON

Approved as to style and content by:


Robert R. Berg
(Chairman of Committee)


W. Douglas Von Gonten
(Member)


James W. Mazzullo
(Member)


John H. Spang
(Head of Department)

August 1986

ABSTRACT

Depositional Environment of the Middle Pennsylvanian
Granite Wash; Lambert 1, Hryhor, and Sundance Fields,
Northern Palo Duro Basin, Oldham County, Texas (August 1986)
Amy Laura Wharton, B.S., The University of Texas at Austin
Chairman of Advisory Committee: Dr. Robert R. Berg

The Lambert 1, Hryhor, and Sundance fields in Oldham County, Texas produce oil from the Middle Pennsylvanian Canyon granite wash. Canyon granite wash conglomerates and sandstones have a total thickness of about 450 feet (137 m) and were derived from granitic rocks of the Bravo Dome. The sediment was transported across carbonate platforms by streams and deposited in the Oldham Trough as fan-deltas. The Oldham Trough is a structural depression east of the Bravo Dome that connects the Palo Duro and Dalhart basins. Granite wash deposits consist primarily of imbricated gravels and cross-stratified sands which are very poorly sorted and have a mean grain size of 1.5 mm. The conglomerates and sandstones are arkoses and consist dominantly of feldspar, granitic rock fragments, and quartz. Carbonate cement averages 5% of the bulk composition. The association of primary and secondary rock properties suggests rapid deposition and shallow burial history.

Six depositional stages for the Middle Pennsylvanian are recognized; 1) Strawn Limestone platform development and progradation, 2) Strawn granite wash progradation, 3) a second Strawn Limestone development due to transgression and basin subsidence, 4) Canyon

Limestone platform development and progradation, 5) Canyon granite wash progradation, and 6) a second Canyon Limestone development due to transgression and basin subsidence, with mound-like buildups occurring on structural highs, and shale filling the Oldham Trough.

The Cisco shales of the Middle and Late Pennsylvanian are the probable source rocks for the Pennsylvanian oil. Temperatures and burial depth were great enough for the shales to generate oil and possibly wet gas. Oil accumulated in structural traps located on upthrown blocks bounded by high-angle reverse and normal faults.

The reservoir conglomerates and sandstones have an average porosity of 18% and an average permeability of 75 md. Calculated water resistivity is 0.028 ohm-meter. Reasonable net pay cutoff values in these granite wash reservoirs are 9.5% for porosity and 1.5 md for permeability.

To my parents
Dr. and Mrs. James Taylor Wharton
and husband
James Burke Vanderhill

ACKNOWLEDGEMENTS

I wish to thank all those people who have contributed to the successful completion of this thesis. My special thanks go to Max E. Banks, President of Baker and Taylor Drilling Co., and Chester Lambert, Vice President who supplied all of the data examined in this study. Mr. Banks and Mr. Lambert gave me four summers of invaluable guidance, support and experience. Their patience and encouragement have guided my career. They will always be greatly appreciated.

Dr. Robert Berg, whom I deeply respect and feel privileged to have had as the chairman of my advisory committee, made this study an enjoyable and rewarding experience. He devoted many hours to helping me solve complicated problems. Dr. Jim Mazzullo willingly shared his expertise in sedimentology and the use of his equipment. Dr. Douglas Van Gonten contributed to the analysis of porosity and permeability. Dr. Thomas Tieh always found time to discuss petrography and diagenesis. The support of these faculty members is gratefully acknowledged.

I want to thank Mr. Foster Twell for his background discussions at the initiation of this project. Thanks are also extended to Mr. Dave Jewell for his help in the interpretation of the seismic data.

I am especially grateful to all of the graduate students at A&M who made my years at the University a rewarding and fun experience. Special thanks to Becky Lambert, Lynne Fahlquist and Anne Linn for their friendship and support. Becky provided constructive advice and ran many errands for me which helped bring this

thesis to a close. I thank Kathy Locke for identification of the trace fossils.

Mrs. Myrna Armstrong's efficiency in typing this thesis is greatly appreciated. Mrs. Sue Baer at Baker and Taylor will always be remembered for her help in gathering data. Lili Lyddon and Robin Connolly are responsible for the professional quality of the drafting.

Finally, I thank my mom and dad for their financial support and encouragement throughout my entire education. My sisters, Tiffany and Nanci always kept me laughing and made the stressful times a little easier. Most of all I thank Jim, my husband, for many helpful discussions and editing. His inspiration and love have made everything worthwhile.

TABLE OF CONTENTS

	Page
INTRODUCTION.....	1
Regional Structure.....	2
Regional Stratigraphy.....	4
Oil and Gas Fields of the Texas Panhandle.....	7
Granite Wash Oil Fields.....	9
Lambert 1, Hryhor, and Sundance Fields.....	9
Tectonic History.....	10
Stratigraphy.....	15
Drilling History.....	20
Methods.....	23
CHARACTERISTICS OF THE GRANITE WASH CONGLOMERATE.....	25
Introduction.....	25
Sedimentary Structures.....	26
Composition.....	35
Texture.....	46
INTERPRETATION.....	48
Introduction.....	48
Alluvial Fan Deposits.....	48
Sediment Source.....	50
Depositional Environment of the Canyon Granite Wash.....	50
Canyon Limestone.....	55
Structural Setting of the Fields.....	60
Lambert 1 Field.....	61
Hryhor Field.....	66
Sundance Field.....	69
Depositional History.....	69
OIL ACCUMULATION.....	76
Oil Source.....	76
Trapping Mechanisms.....	80
Log Interpretation.....	81
Reservoir Properties.....	90
CONCLUSIONS.....	103
REFERENCES CITED.....	105
APPENDIX I.....	110
APPENDIX II.....	113

TABLE OF CONTENTS (continued)

	Page
APPENDIX III.....	114
APPENDIX IV.....	123
APPENDIX V.....	124
APPENDIX VI.....	128
APPENDIX VII.....	131
VITA.....	134

LIST OF FIGURES

Figure		Page
1	Structural elements of the Texas Panhandle.....	3
2	Regional structure map drawn on the top of the Precambrian basement.....	11
3	Structure map drawn on the top of the Canyon granite wash conglomerate.....	14
4	Generalized stratigraphic cross section A-A' showing the correlation of the Canyon granite wash conglomerated from the Bravo Dome to the Oldham Trough.....	18
5	Gamma-ray and resistivity log response of the Granite Wash Conglomerate, Aurora 1 (H12), Hryhor field.....	19
6	Sedimentary structures in vertical sequence of the Canyon granite wash conglomerate in the Jay Taylor B-1 (L2) core.....	28
7	Sedimentary structures in vertical sequence of the Canyon granite wash conglomerate in the Parker Creek 1 (S27) core.....	32
8	Sedimentary structures in vertical sequence continued from Figure 7, Parker Creek 1 (S27) core.....	34
9	Logarithm of rock fragment (Rx)-to-feldspar (F) ratio versus logarithm of mean grain size.....	38
10	Maximum and mean grain size and generalized composition plotted with gamma-ray and resistivity logs.....	40
11	Maximum and mean grain size and generalized composition plotted with gamma-ray and resistivity logs.....	41
12	Photomicrographs of the Canyon granite wash conglomerate in the Jay Taylor B-1 (L2) core taken at 25X power.....	44
13	Gross isopach of the Canyon granite wash interval in the Lambert 1, Hryhor, and Sundance fields showing the trend and morphology of the granite wash lenses.....	54
14	Net isopach of the Canyon granite wash interval in the Lambert 1, Hryhor, and Sundance fields showing the distribution of clean granite wash using a cutoff of 225 API units on the gamma-ray log.....	57

LIST OF FIGURES (continued)

Figure	Page	
15	Isopach of the Canyon Limestone interval in the Lambert 1, Hryhor, and Sundance fields showing the carbonate platform margin.....	59
16	Migrated 12-fold seismic section showing the two high-angle reverse faults which form the boundaries of the Sundance and Hryhor fields.....	63
17	Stratigraphic cross-section B-B' showing the vertical and lateral variation of the Canyon granite wash in the Lambert 1 Field.....	65
18	Stratigraphic cross-section C-C' showing the vertical and lateral variation of the Canyon granite wash across the study area.....	68
19	Stratigraphic cross-section D-D' showing the vertical and lateral variation of the Canyon granite wash in the Sundance field.....	71
20	Diagrammatic cross-section from the Bravo Dome to the Oldham Trough showing the depositional history of the Canyon and Strawn sediments in the study area.....	73
21	Lopatin diagram illustrating the burial history of the Cisco Shale and its relation to hydrocarbon generation, Oldham Trough, Northern Palo Duro basin.....	78
22	Core analysis showing porosity, permeability and fluid saturations in the Canyon granite wash interval, Jay Taylor B-1 (L2), Lambert 1 Field.....	83
23	Cross plot of porosity and bulk density from the Jay Taylor B-1 (L2) showing estimated bulk density of the Canyon granite wash.....	85
24	Cross plot of permeability and porosity from the Jay Taylor B-1 (L2) core (Figure 23) showing bimodal distribution of porosity.....	87
25	Pickett plot for Jay Taylor B-1 (L2) well showing water resistivity (R_w) of 0.025 ohm-m and variations in water saturation (S_w).....	88

LIST OF FIGURES (continued)

Figure		Page
26	Pickett plot for Fulton King A-2 (L5) well showing water resistivity (R_w) of 0.028 ohm-m and variations in water saturation (S_w).....	89
27	Classification of porosity data into ranges of 1 percent porosity for all samples from the Jay Taylor B-1 (L2) core.....	92
28	Classification of porosity data into ranges of 1 percent porosity for all samples from the Parker Creek 1 (S27) core.....	94
29	Calculation of porosity distribution from classified data for determination of cumulative capacity for the Jay Taylor B-1 (L2) core.....	97
30	Calculation of porosity distribution from classified data for determination of cumulative capacity for the Parker Creek 1 (S27) core.....	99
31	Classification of permeability data into equal logarithmic intervals.....	102

LIST OF TABLES

Table		Page
1	Stratigraphic section for the Paleozoic of the Oldham Trough, Oldham County, Texas Panhandle (modified from Handford and Dutton, 1980).....	16
2	Cumulative production, April 1985, and average reservoir characteristics, Canyon Granite Wash, Oldham Trough, Northern Palo Duro Basin, Texas Panhandle.....	21
3	Canyon Granite Wash completion records, Lambert 1, Hryhor, and Sundance fields, Oldham County, Texas Panhandle.....	22
4	Average compositional and textural properties of the Canyon granite wash from the Jay Taylor B-1 (L2) and the Parker Creek 1 (S27) cores, Oldham County, Texas.....	36
5	Calculation of time-temperature index (TTI) for burial history of the Cisco Shale in Figure 21.....	79
6	Average porosities and permeabilities for the Canyon granite wash, Lambert 1 and Sundance fields, Oldham County, Texas. Interval footage corresponds with core descriptions (Appendix III).....	82
7	Calculation of Granite wash bulk density.....	86

INTRODUCTION

The Middle Pennsylvanian granite wash is a substantial oil and gas reservoir in the Texas Panhandle. The term "granite wash" refers to sandstone derived from a nearby granitic source (Flawn, 1965). No surface exposures of Pennsylvanian granite wash occur in the study area, and therefore its study depends on subsurface data: the primary rock properties observed in cores, core analysis, electric logs, drill stem tests, dip logs, and seismic records.

Five granite wash fields have been discovered adjacent to the Bravo Dome in Oldham County, Texas; the Lambert 1, Hryhor, Sundance, Pond, and Brandi. The section at Lambert 1, Hryhor, and Sundance fields, which is the focus of this thesis, consists of granitic rock fragments, feldspathic sandstones, and silty mudstones, interbedded with limestones and shales.

The objectives of this study are interpretation of the depositional environment of the granite wash, and determination of reservoir geometry and properties. This study is undertaken in order to explain the origin of the reservoirs, to aid in log interpretation, and to facilitate future prospecting for other granite wash reservoirs in the Texas Panhandle.

This thesis follows the style and format of the American Association of Petroleum Geologists Bulletin.

Regional Structure

The major positive structural features of the Texas Panhandle consist of the Amarillo Uplift, Bravo Dome, and Matador Arch (Figure 1). The basins include the Anadarko, Dalhart and Palo Duro. The Amarillo Uplift covers 4 counties and extends into 8 others. It is dominated by a northwest-southeast granitic core that comes to the surface in Oklahoma to form the Wichita Mountains (Roth, 1949). The Bravo Dome is an eastern extension of the Sierra Grande Uplift (Kluth and Coney, 1981) and occupies central and western Oldham county. The Matador Arch separates the Palo Duro and Midland basins.

The Anadarko basin is bounded on the north by broad, flat cratonal shelf areas, on the south by the Amarillo Uplift, and on the west by the Cimarron Arch (Evans, 1979; Pippin, 1970; Adler et al., 1971). The basin occupies 6 counties in the eastern Texas Panhandle and extends into 5 other Texas counties. However, most of the basin is in Oklahoma. The Anadarko is approximately 30,000 feet (9150 m) deep (Budnik and Smith, 1982), with a northwest-southeast trending axis adjacent to the Amarillo Uplift (Nicholson, 1960). The boundary between the Amarillo Uplift and the basin is a complicated zone of folds and faults (Adler et al., 1971).

The asymmetric Palo Duro basin is bounded on the northeast by the Amarillo Uplift, on the northwest by the Bravo Dome, and on the south by the Matador Arch. It occupies approximately 14 counties in the southern Panhandle. It is a relatively shallow basin, approximately 11,000 feet (3354 m) deep, and maximum Pennsylvanian deposition occurred along a northwest trending axis (Dutton, 1980a).

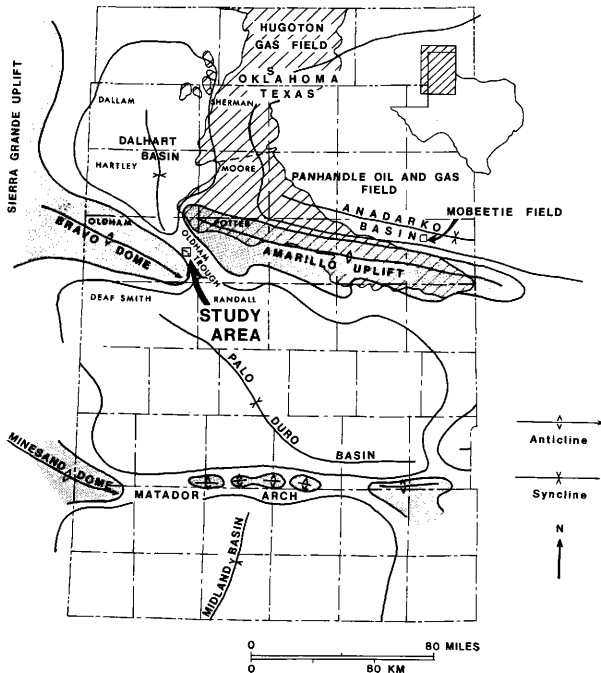


Figure 1. Structural elements of the Texas Panhandle. Major structural highs are shaded. The Panhandle Oil and Gas field and the Hugoton Gas field are striped. The study area and Mobeetie field are indicated by arrows (modified from Nicholson, 1960; Pippin, 1970).

The Dalhart basin is a northwestern extension of the Palo Duro basin (Roth, 1949), and is bounded on the west by the Sierra Grande Uplift and on the east by the Cimarron Arch. It occupies 2 counties in the northwest Panhandle and approximately half of Cimarron county in Oklahoma. The Dalhart basin is also relatively shallow, 10,000 to 12,000 feet (3050 to 3680 m) deep (Budnik and Smith, 1982) and is less structurally complex than the Anadarko basin (Adler et al., 1971).

These structural features controlled the areas of erosion and deposition from the early Pennsylvanian through the Permian. The uplifts eventually formed barriers to seaways that connected the basins, and resulted in the formation of barred and landlocked basins (Rogatz, 1935). Restricted seaway circulation and dry climatic conditions in the Permian produced the evaporite sequences which seal the Pennsylvanian sediments.

Regional Stratigraphy

The Anadarko basin contains rocks representing most of the Paleozoic Era (Evans, 1979). They are approximately 20,000 feet (6098 m) thick in the Texas Panhandle and reach a maximum thickness of 40,000 feet (12,195 m) in Oklahoma (Adler et al., 1971). The basin is a significant oil and gas province. The most important reservoir rocks for oil and gas accumulation, in order of importance, have been; the Pennsylvanian sandstones and limestones; the Middle Ordovician sandstones and carbonates; the Mississippian carbonates; the Lower Ordovician limestones; and the Silurian carbonates. Both structural and stratigraphic traps are important.

The Cambrian in the Anadarko basin consists of the Reagan Sandstone. The Ordovician system comprises the Arbuckle Limestone and Simpson Group sandstones, and the Viola Limestone and Sylvan Shale. The Siluro-Devonian consists of the Hunton Group limestones. The Mississippian contains the Kinderhookian, Osagian, Meramecian, and Chesterian. The Pennsylvanian system comprises the Springerian in the eastern part of the basin and also, the Morrowan, Atokan, Des Moinesian, Missourian, and Virgilian series occur throughout the basin. The Permian contains the Wolfcampian, Leonardian and Guadalupian series. Triassic, Tertiary, and Quaternary strata unconformably overlie the Permian. Other unconformities are recognized at the base of the Silurian, Mississippian, Triassic, Tertiary, and Quaternary (Committee of Panhandle Geological Soc., 1955).

The Palo Duro basin contains approximately 13,700 feet (4177 m) of Paleozoic age rocks (Birsá, 1977). The sequence has good reservoir rocks, a high organic content, and abundant traps and seals. However, the basin generally lacks production except around the margin. It has been suggested that the geothermal gradient may have been too low for significant amounts of hydrocarbons to be generated (Dutton, 1980b; Fritz, 1986).

The Cambrian basal Hickory sandstone in the Palo Duro basin is relatively thin and is restricted to the south central and eastern portion of the basin (Birsá, 1977). The Ordovician consists of approximately 550 feet (168 m) of Ellenburger limestone. The Silurian and Devonian are absent due to erosion and non-deposition (Dutton, 1980a). The Mississippian contains Osagian, Meramecian, and Chesterian rocks

which are simply referred to as the Mississippi lime. The Mississippi lime is approximately 450 feet (137 m) of light-colored carbonates (Birska, 1977). All of the Pennsylvanian series are present and account for approximately 4,400 feet (1341 m) of the sequence. The lithologies are highly variable and contain shale, limestone, red beds, sandstone, and granite wash. The Permian is the thickest sequence of sediments found in the Palo Duro basin, and is approximately 7500 feet (2287 m) thick. The Wolfcampian is primarily carbonate and shale. The Leonardian and Guadalupian contain evaporite, red beds, and some sandstone. Triassic, Tertiary, and Quaternary strata unconformably overlie the Permian System. Other major unconformities are at the base of the Cambrian, Ordovician, Mississippian, and Pennsylvanian (Birska, 1977).

The Dalhart basin is stratigraphically similar to the Palo Duro because it was a northern extension of the basin (Dutton, 1980a). It contains the same sequence of rocks as the Palo Duro with the following exceptions and different thicknesses (McCasland, 1980). The Ordovician also contains the Simpson sandstones and dolomites, and the Viola limestone. The Mississippian also contains the Kinderhook sandstones with interbedded dolomite. The Wolfcampian sediments reach a total thickness of more than 5000 feet (1524 m), and average between 800 and 2100 feet (243 and 640 m) (McCasland, 1980). Triassic, Jurassic, Cretaceous, Tertiary and Quaternary strata unconformably overlie the Permian system. Other major unconformities are equivalent to those in the Palo Duro basin.

Oil and Gas Fields in the Texas Panhandle

The Panhandle Oil and Gas Field is the major reservoir in the Texas Panhandle (Figure 1). Gas was first discovered in 1918, in Potter County at a depth of 2,600 feet (793 m) (Rogatz, 1935), and oil was discovered in 1921 at a depth of 2,900 feet (884 m). Lithologies of Wolfcampian age that produce oil and gas are dolomite, limestone, sandstone, granite wash, and weathered granite. Local names of the producing horizons are; Brown Dolomite, White Dolomite, Moore County Lime, Arkosic Dolomite, Arkosic Lime, and Granite Wash.

Uplift of the Amarillo mountains during the Atokan caused the south edge of the Anadarko basin to shift northward producing a reversal of dip direction from west to southeast (Pippin, 1970). The northwest-southeast trending granitic core was exposed and erosion resulted in the deposition of granite wash northeast into the Anadarko basin and southwest into the Palo Duro basin (Rogatz, 1935). Granite wash interbedded with marine muds and carbonate filled the Anadarko basin and the uplift was covered by Wolfcampian time. Southeast tilting of the Anadarko during the Cretaceous caused updip wedging of Permian and Pennsylvanian sediments which formed the trap along the west edge of the Panhandle and Hugoton fields (Pippin, 1970). The evaporitic Wichita Formation formed a seal over the Wolfcampian reservoir beds. The Panhandle field is an anticlinal trap whose southeastern part has a steep structural dip which gradually decreases to the northwest. The steep dip has caused the gas, oil and water columns to cut across formation boundaries (Pippin, 1970). Progressively older reservoirs are found in the updip direction. Formation

water moves downdip and west to east causing a hydrodynamic tilt of the gas-water contact (Pippin, 1970).

The northern extension of the Panhandle field is often referred to as the Hugoton gas field (Figure 1), and is a large stratigraphic trap. The Herington and Krider formations produce gas and are equivalent to the Brown Dolomite in the Texas Panhandle. Reservoir beds thin updip and pinch-out westward. The updip point where the reservoirs produce only water appears to be determined by an abrupt local change of porosity and permeability. However, the critical trapping mechanism is the southeastward, downdip dynamic flow of formation water (Pippin, 1970).

Oil production in the Texas Panhandle covers 300,000 acres, extending approximately 125 miles (202 km) in parts of 5 Texas counties, and gas production in the Panhandle and Hugoton fields covers 5,000,000 acres, extending approximately 50 miles (81 km) in Texas and 110 miles (177 km) in Oklahoma and Kansas (Rogatz, 1935). The American Petroleum Institute's original oil-in-place estimates as of December 31, 1979 were 6,060,000,000 barrels. Estimated cumulative production was 1,333,374,000 barrels. Ultimate recovery of natural gas for the Texas panhandle was 55,835,860 million cubic feet (American Petroleum Institute, 1980).

The Pennsylvanian Morrow Sandstone is also a significant oil reservoir in the Texas Panhandle. Oil is produced from more than 60 fields in Texas with many additional fields in Oklahoma, Kansas, and Colorado (Galloway et al., 1983). The two most productive fields in Texas are both in Ochiltree County. The Texas panhandle fields

have a cumulative production of more than 40 million barrels that has been produced from deltaic and fluvial sandstones of the Morrow (Galloway et al., 1983).

Granite Wash Oil Fields

Granite wash reservoirs adjacent to the Amarillo Uplift have been compared to modern alluvial fans. Dutton (1982) interpreted the granite wash reservoirs at Mobeetie field, Wheeler County (Figure 1) as ancient fan deltas, or alluvial fans that prograded into a body of water from an adjacent highland. Granite wash is found near the flanks of uplifts, with shales and sandstones a short distance away and shales and thin limestones basinwards (Dutton, 1980a).

Lambert 1, Hryhor, and Sundance Fields

Granite wash reservoirs have also been discovered adjacent to the Bravo Dome in Oldham County. A narrow, northwest trending trough connects the Dalhart and Palo Duro basins in eastern Oldham and western Potter counties, Texas (Dutton, 1980a) (Figure 2). The study area is located within this trough, approximately 12-15 miles (19-24 km) northeast of Vega, Texas. The trough is bounded on the west by the Bravo Dome and on the east by the Amarillo Uplift. The intervening low is referred to here as the Oldham trough.

Tectonic History. The crystalline basement in the Texas Panhandle consists of Precambrian igneous rocks (Figure 2). Muehlberger et al., (1976) referred to the basement complex underlying the granite wash in the study area as the "Panhandle Volcanic Terrane" and gave an age of 1100-1200 Ma. The Pennsylvanian granite wash was deposited directly above weathered Precambrian basement in the Oldham trough. The Palo Duro Basin contains Cambrian and Ordovician rocks whose absence in the Oldham trough is probably due to pre-Pennsylvanian erosion. Mid-Ordovician to early Mississippian rocks are also absent. Adams (1954) postulated that a northwest trending extension of the Transcontinental Arch, the Texas Peninsula, separated the West Texas and Oklahoma embayments and prevented mid-Ordovician to Early Mississippian deposition on the crest of the low lying arch. By early Mississippian time, the Peninsula ceased to be a positive element and younger Paleozoic beds were deposited over it.

The Dalhart basin and the Palo Duro basin were initiated in the Late Mississippian during development of the Amarillo Uplift and associated folding, which began in the mid-Devonian (Nicholson, 1960). The Sierra Grande Uplift and Bravo Dome began to form in Morrow-Atokan time (Birsá, 1977). Uplift of the Amarillo Mountains was accomplished primarily by large-scale block faulting, which produced relatively high, rugged land masses, similar to those of the Ancestral Rocky Mountains. Development of the intracratonic basement uplifts may have been the result of the complex intraplate response to the collision of North America with South America-Africa (Kluth and Coney, 1981). Both the Amarillo Uplift and Bravo Dome are consi-

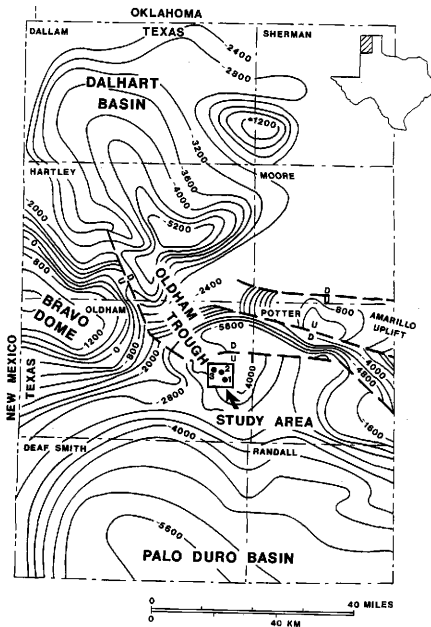


Figure 2. Regional structure map drawn on the top of the Precambrian basement. Contour interval is 400 feet. Study area consists of three oil fields, designated by number; Lambert 1 (1), Hryhor (2), and Sundance (3) (modified from Dutton and others, 1979).

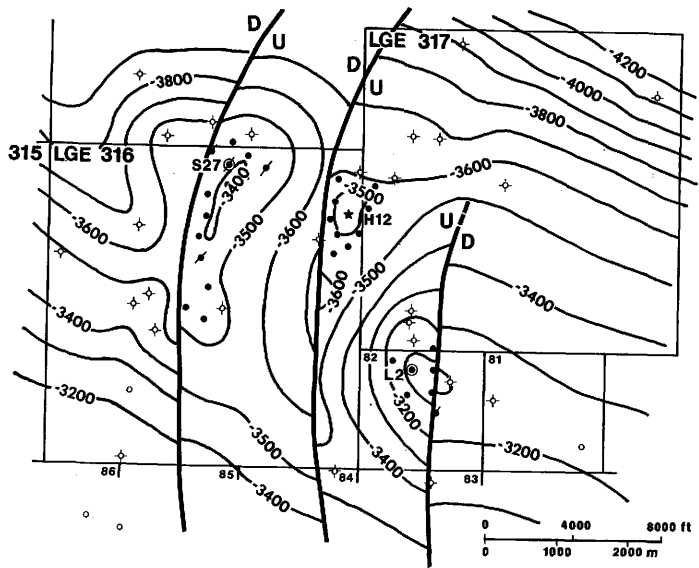
dered to be the major contributors of granite wash in the Texas Panhandle during the Pennsylvanian.

Intense weathering of exposed granite highlands during the Early and Middle Pennsylvanian resulted in granite wash accumulations on adjacent slopes in many of the basins and troughs in Colorado, Oklahoma, New Mexico, and Texas. During the Pennsylvanian the study area was located approximately 10-11° north of the equator (Schopf, 1975). The hot, humid climate contributed to the rapid weathering of the granite highlands. The Mobeetie field of Wheeler County, Texas (Dutton, 1982) produces oil from coarse-grained conglomerates shed from the Amarillo Uplift. Erosion of the granite core of the Pedernal Uplift in southeastern New Mexico provided coarse-grained clastics to the Permian and Orogrande basins (Meyer, 1966).

The Lambert 1, Hryhor, and Sundance fields lie just east of the Bravo Dome. High structural relief, produced by Precambrian faulting, combined with an impermeable seal of shale or limestone, resulted in the formation of the hydrocarbon reservoirs (Figure 3).

Following deposition of the Pennsylvanian, Permian, Triassic, and Jurassic, the Panhandle was possibly covered with Cretaceous marine sediments. Erosion has eliminated most evidence (Eddleman, 1961), but remnants of Cretaceous rocks have been identified in the Palo Duro Basin (Dutton and others, 1979). Movement along pre-existing faults was renewed by the Late Cretaceous Laramide orogeny. The late Miocene-Pliocene Ogallala Formation was deposited across the entire area.

Figure 3. Structure map drawn on the top of the Canyon granite wash conglomerate. Contour interval is 100 feet. Cored wells are circled. The type log is from the H12 well and indicated as a star.



Stratigraphy. The Lambert 1, Hryhor, and Sundance fields contain Early and Middle Pennsylvanian conglomerates and coarse-grained sandstones which were eroded from the exposed Bravo Dome and trapped in the Oldham trough. The section unconformably overlies Precambrian basement rock (Table 1). Carbonates were deposited intermittently, interfingering with the clastic deposits (Figure 4). Canyon granite wash was transported across the carbonate buildup and deposited on the slope. A typical log response for the lower Pennsylvanian section is shown in Figure 5. Informal formation names used in the study area do not necessarily correlate exactly to the Canyon and Strawn groups.

Carbonate deposits developed around the margins of the Palo Duro and Dalhart basins during the Pennsylvanian (Birsá, 1977). The ridge of the Amarillo Uplift was probably sufficiently high to resist marine inundation from Late Mississippian until Early Permian time (Eddleman, 1961), while the Bravo Dome and stable shelf areas of the north and northwest Panhandle were covered earlier. Fine clastics accumulated in the center of the basins. Subsidence and renewed carbonate deposition followed in the Early Permian.

The Palo Duro and Dalhart basins were filled by the end of Wolfcampian, and the seas became landlocked (Eddleman, 1961). Evaporitic dolomite, anhydrite, and salt with interbedded red and green shales were formed throughout the remainder of the Permian, Triassic, and Jurassic. Due to the Laramide orogeny, at the end of the Cretaceous, no marine deposits younger than Permian are known in the Panhandle area (Nicholson, 1960). The Texas Panhandle has

Table 1. Stratigraphic section for the Paleozoic of the Oldham Trough, Oldham County, Texas Panhandle (modified from Handford and Dutton, 1980).

Era	System	Series	Group	Informal formation name	General Lithology and depositional setting
Paleozoic	Permian	Leonardian	Clear Fork	Tubb	red beds, anhydrite, and peritidal dolomite
				Red Cave	
			Wichita	Panhandle Limestone	
			Wolfcampian	Brown Dolomite	
	Pennsylvanian		Virgilian	Cisco	Limestone and shale Cisco shale
			Missourian	Canyon	Canyon Limestone
					Canyon Granite Wash
			DesMoinesian	Strawn	Strawn Limestone
					Strawn Granite Wash
Precambrian	Complex of Intrusives		Basement	granite	

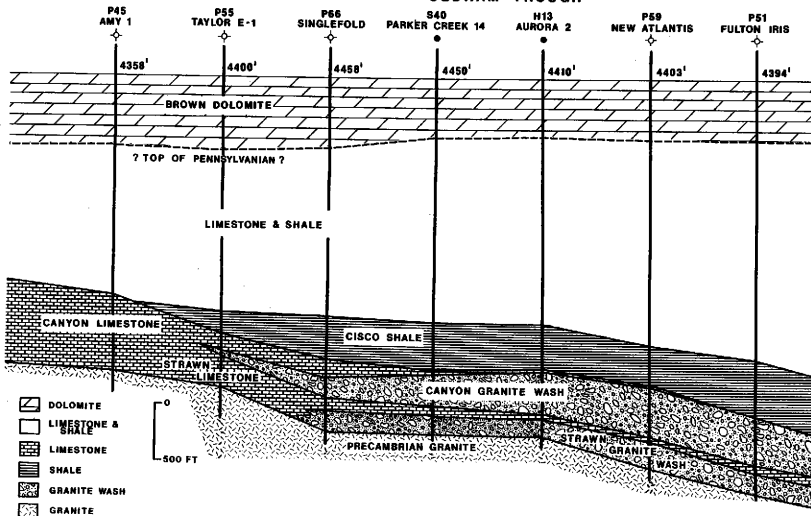
Figure 4. Generalized stratigraphic cross section A-A' showing the correlation of the Canyon granite wash conglomerate from the Bravo Dome to the Oldham Trough. The datum is the top of the Brown Dolomite. The Brown Dolomite Formation is denoted as a zone of dolomite for simplicity. However, the zone contains several lithologies. Line of section shown in Appendix II.

A
SW

A
NE

BRAVO DOME

OLDHAM TROUGH



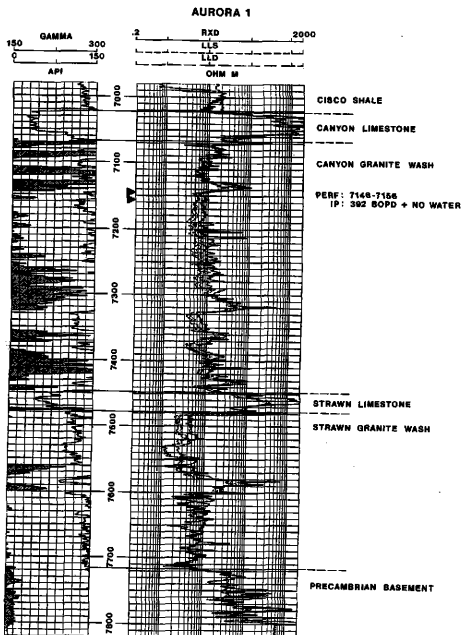


Figure 5. Gamma-ray and resistivity log response of the Granite Wash Conglomerate, Aurora 1 (H12), Hryhor field. Diagram shows the informal formation names used in mapping the fields. Location of well is shown in Figure 3.

been tectonically inactive since early Tertiary time.

Drilling History. Baker and Taylor Drilling Company discovered oil in the Canyon Granite Wash in Section 82, Block GM-5, State Capitol Lands Survey, Oldham County, Texas in December, 1978. Evaluation of electric logs led to the re-entry of a previously plugged well. The Jay Taylor A-1 (L1) was perforated at 6776-6786 feet (2066-2069 m) and treated with 500 gallons of acid. The initial production was 477 barrels of oil/day with an API gravity of 42.8°. Successful completion initiated the development of the Lambert 1 field.

Due to the success of the Lambert 1 field, numerous seismic surveys were run from 1979 through 1983. Interpretation of structural highs, and normal and high-angle reverse faults led to the discovery of two additional fields, the Sundance (1981) and the Hryhor (1982). Many additional wildcat wells were drilled on fault bounded structures interpreted from seismic records. The Pond and Brandi fields were discovered in 1983.

The Lambert 1, Hryhor, and Sundance fields are structural traps (Figure 3). The depositional and tectonic history greatly influence reservoir quality (Table 2). As of August, 1985, the Lambert 1 field leads in cumulative production with 1.8 million barrels of oil. The Hryhor and Sundance fields have produced 1.2 million and 1.0 million barrels of oil respectively (Table 3). Maximum thickness of the Canyon granite zone is 497 feet (151 m) and is encountered at approximately 7250 feet (2210 m) in the Aurora 12 (H23) well. Estimated total reserves for the three fields is 6 million barrels of oil.

Table 2. Cumulative production, April 1985, and average reservoir characteristics, Canyon Granite Wash, Oldham Trough, Northern Palo Duro Basin, Texas Panhandle.

Field	Average Porosity %	Average Permeability (Md)	Water Saturation %	Oil Gravity ($^{\circ}$ API)	Average Oil Zone Thickness (ft)	Number of producing wells	Area (acres)	Cumulative production (Mbbbl)	Estimated Total Reserves (Mbbbl)
Lambert 1	15	86	48.0	41.5	87	6	175	1.8	2.5
Hryhor	17	67	44.5	43	35	12	259	1.2	2.2
Sundance (includes Neptune 1 well)	19.3	45	45.0	42	38	9	211	1.0	1.3

Estimated total reserves figures from a study by Kepfinger, Inc., April 1985.

Table 3. Canyon Granite Wash completion records, Lambert 1, Hryhor, and Sundance fields, Oldham County, Texas Panhandle.

Field	Well	Well Symbol	Completion Date (month-year)	Top Can GM (ft)	Subsea (ft)	Perforated Interval	Initial Production		Daily Production February-1986		
							Oil bbls/day	Meter bbls/day	Oil bbls/day	Meter bbls/day	
Lambert 1	Jay Taylor A-1	L1	1-79	6768	-3151	6776-6786	477	0	3	297	
	Jay Taylor B-1	L2	3-79	6678	-3078	6707-6760	555	0	47	164	
	Jay Taylor D-1	L3	6-79	6826	-3174	6945-6880	296	58	0	302	
	Fulton-King A-1	L4	4-79	6654	-3054	6655-6730 6740-6750	576	0	162	142	
	Fulton-King A-2	L5	4-79	6644	-3067	6635-6660 6670-6720	556	0	48	91	
	Fulton-King A-3	L6	5-79	6750	-3150	6760-6800	249	14	48	190	
Hryhor	Aurora 1	H12	3-82	7066	-3482	7146-7156	392	0			
			1-86		Plugged Back	7057-7130			181	3	
	Aurora 2	H13	4-82	7090	-3500	7168-7176	454	38	87	213	
	Aurora 3	H14	4-82	7075	-3508	7152-7158	585	26	6	144	
	Aurora 4	H15	5-82	7052	-355	7140-7148	464	0	137	71	
	Aurora 6	H17	5-82	7125	-3550	7124-7152	564	0	149	151	
	Aurora 7	H18	5-82	7084	-3533	7080-7122	755	0	14	151	
	Aurora 8	H19	5-82	7130	-3517	7202-7207	250	33	18	130	
	Aurora 9	H20	5-82	7155	-3580	7156-7160	223	66	0	141	
	Aurora 10	H21	5-82	7080	-3517	7080-7150	636	3	192	0	
	Aurora 11	H22	6-82	7100	-3562	7100-7115	545	0	101	138	
	Aurora 13	H24	8-82	7098	-3530	7092-7140	582	0			
				5-85		Plugged Back	7092-7095			31	86
	Aurora 15	H26	10-82	7126	-3567	7120-7140	418	0	5	161	
	Sundance	Parker Creek 1	S27	8-81	7010	-3407	7020-7058	666	0	Shut In	1-86
Parker Creek 2		S28	11-81	7018	-3405	7032-7048	358	0	59	232	
Parker Creek 3		S29	11-81	7006	-3430	7008-7034	390	0	2	295	
Parker Creek 4		S30	12-81	7039	-3404	7050-7106	297	0	38	202	
Parker Creek 6		S32	2-82	7060	-3390	7076-7134	389	0	6	159	
Parker Creek 7		S33	3-84	7025	-3445	7031-7042 7048-7058 7065-7070	4	27	Shut In	7-85	
Parker Creek 8		S34	2-82	7078	-3438	7078-7112	366	0	17	225	
Parker Creek 10		S36	3-82	7122	-3445	7134-7140	168	75	Shut In	10-84	
Parker Creek 11		S37	3-82	7100	-3440	7126-7140	168	23	Shut In	7-83	
Parker Creek 12		S38	6-82	7103	-3413	7106-7164	380	0	31	125	
Parker Creek 13		S39	9-82	7090	-3406	7096-7162	566	0	38	78	
Parker Creek 14		S40	3-84	7150	-3457	7158-7156	9	299	Shut In	7-84	
Parker Creek 15		S41	10-82	7170	-3485	7168-7176	163	24	4	36	
Neptune 1		N42	6-82	7097	-3439	7093-7119	572	5	40	167	
Neptune 3		N44	3-84	7157	-3465	7142-7144 7158-7160	6	37	Shut In	7-85	

Methods

Interpretation of the depositional environment at Lambert 1 and Sundance fields was based on the examination of full diameter cores from two wells, the Jay Taylor B-1 (L2) and the Parker Creek 1 (S27). The locations of these wells are circled in Figure 3. The slabbed cores were photographed and fully described to establish the vertical sequence of sedimentary structures, texture, and gross composition.

A petrographic analysis was conducted on thin sections taken from representative intervals, normal to bedding. The analysis was made according to standard techniques. The grain size was determined by long axis measurements of 100 detrital grains. The composition was determined for each sample by a point count of 100 grains. Size influenced composition percentages; therefore, the gravels (> 2 mm) were separated from the sands (< 2 mm). Results are presented as a percentage of the total composition. The detrital grains were classified as monocrystalline quartz, feldspar, rock fragments (including polycrystalline quartz), other grains, and matrix (including clay and chlorite). Percentages were normalized after subtracting cement and thin section porosity. Commercial core analyses by Core Laboratories, Inc. provided porosity and permeability measurements.

The reservoir was mapped using logs from 65 wells. The logs were interpreted to define formation boundaries, estimate shale content, and calculate porosities. Shale content was estimated from the gamma-ray log. All beds within the Canyon granite wash interval with API units greater than 225 were counted as shale. Cross sections

were constructed across the study area, and structure and isopachous maps were drawn to determine the morphology and structural configuration of the reservoir. Seismic data were interpreted to define faults.

Porosity and permeability data were classified and evaluated in order to describe the average properties of the reservoir (Amyx, et al., 1960). Porosity versus bulk density was plotted from core analysis and log data to estimate grain density. True resistivity versus porosity plots were constructed to determine water saturation values (Pickett, 1966).

CHARACTERISTICS OF THE CANYON GRANITE WASH CONGLOMERATE

Introduction

The Canyon granite wash sediments at the Lambert 1 and Sundance fields do not fall into any well-ordered pattern on a local scale. However, for descriptive purposes, the sediments can be divided into four general facies; conglomerate, sandstone, mudstone, and shale. In 140 feet (43 m) of core from the Jay Taylor B-1 (L2) well, approximately 23% is conglomerate, 75% sandstone, less than 1% mudstone, and 1% shale. The 42 feet (13 m) of core from the Parker Creek 1 (S27) well contains approximately 5% conglomerate, 20% sandstone, 69% mudstone, and 6% shale. Facies are differentiated by their primary rock properties; sedimentary structures, composition, and texture. These properties can be used to interpret the environment of deposition and transport mechanisms.

The L2 and S27 cores contain a variety of sedimentary structures; pebble imbrication, cross-stratification, parallel lamination, convoluted lamination and soft-sediment deformation. The contacts between the four facies and their associated sedimentary structures occur apparently at random, and no ordered vertical sequence can be established for these cores. Bed set boundaries are difficult to identify. The most common sedimentary structure observed in the vertical sequence of the L2 core is cross-stratification of very coarse to fine-grained sandstone. The S27 core is dominated by mudstone, in which the most common structures are convoluted lamination and other soft-sediment deformation features.

Trace fossils and fossils are scarce, but several types are present in the silty mudstones and shales of both cores.

Composition is highly variable. Percentages of rock fragments, feldspar, and quartz are dependent on grain size. Beds containing more gravel have a higher rock fragment percentage, and beds containing less gravel have a higher feldspar percentage.

The texture is also variable, but is dominated by very poorly-sorted, angular and loosely-packed conglomerate and coarse-grained sandstone.

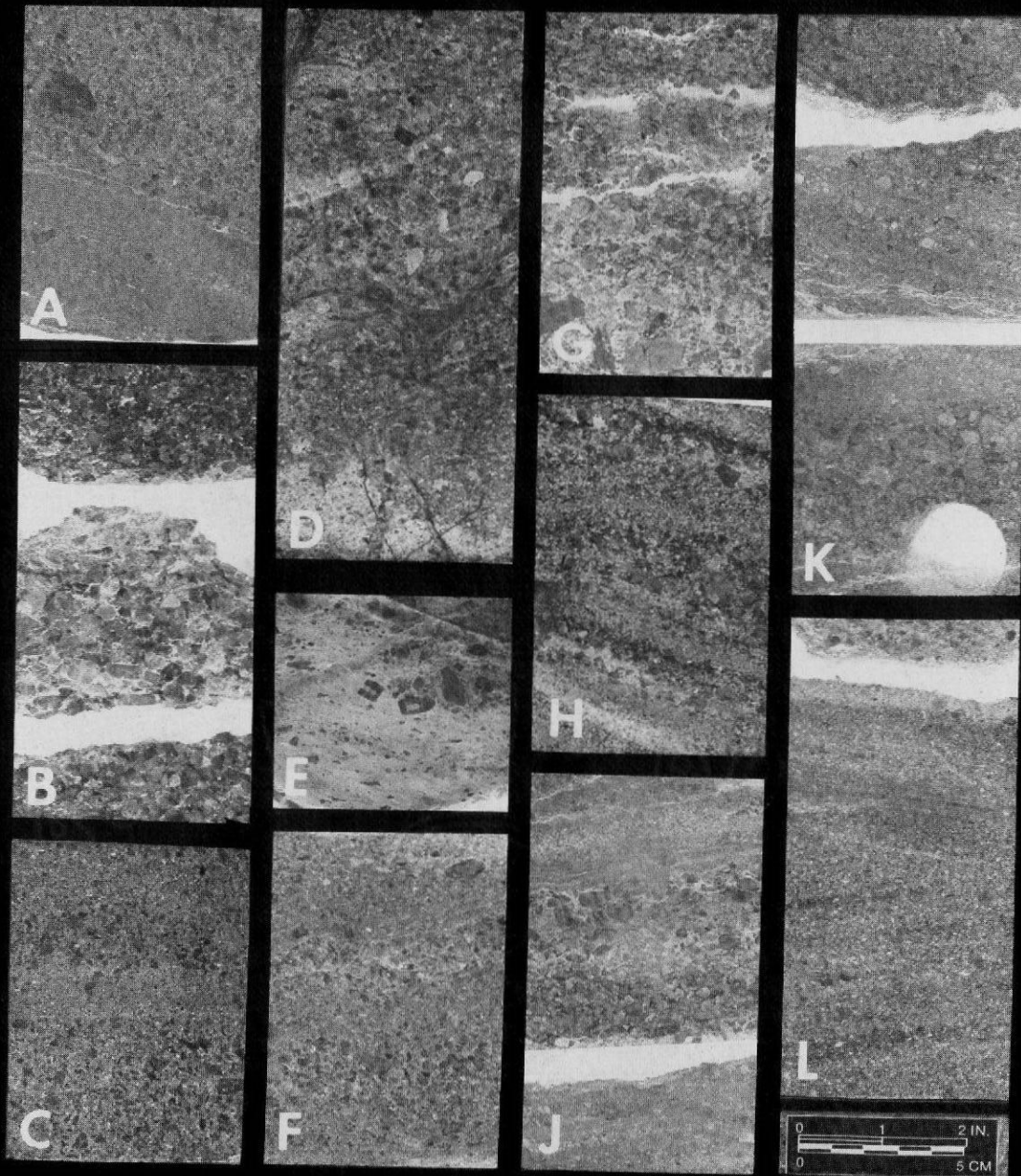
Sedimentary Structures

The conglomerate facies contains the fewest sedimentary structures. Conglomerates are of two types; structureless gravel beds and imbricated gravel beds. The two types occur in variable vertical sequences 4 to 10 feet (1.2 to 3.1 m) thick. Internal lamination is not discernable in the structureless gravel beds (Figure 6-B). This may be the result of the grain size being too large to allow sedimentary structures to be seen in the slabbed face of the 4-inch diameter core. Lack of fabric could also have been caused by rapid deposition (Blatt, et al., 1980). Shale clasts are observed in the L2 core compressed between pebble grains (Figure 6-G). They are identified as clasts because they are discontinuous lenses with irregular thicknesses and outlines.

The imbricated gravel beds contain pebbles with their long axes oriented in the same direction. Orientation of the pebble grains is produced by high flow intensities or mass emplacement

Figure 6. Sedimentary structures in vertical sequence of the Canyon granite wash conglomerate in the Jay Taylor B-1 (L2) core. The boldface letters in the lower left corner of the photographs refer to the captions below.

- A. 6756 feet; sharp inclined contact between fine- to medium-grained sandstone below and pebbly sandstone above. Bedding in the fine- to medium-grained sandstone is inclined 18° . The pebble in the structureless pebbly sandstone is 24 mm in long axis diameter.
- B. 6759 feet; structureless gravel, poorly-sorted, loosely-packed, patchy cement, pebbles are angular, fine-grained sand and silt matrix, lack of stratification features.
- C. 6787 feet; fine- to medium-grained sandstone shows parallel, even, horizontal laminae, which are in alternating 20-40 mm bands.
- D. 6794 feet; tightly cemented very coarse-grained to pebbly sandstone, dolomite cemented fractures.
- E. 6796 feet; rock fragments and broken and fragmented crinoid stems, suspended in silty mudstone. Coarse-grained sand shows wavy flow pattern.
- F. 6812.5 feet; cross-stratified fine- to coarse-grained pebbly sandstone, poorly-sorted, containing multidirectional trough or planar cross-bedding with a truncation surface. Pebble in upper right corner is 11 mm in long axis diameter.
- G. 6813 feet; structureless gravel, poorly-sorted, interbedded with compressed shale clasts. Pebble at base of photo is 18 mm in long axis diameter.
- H. 6823 feet; cross-stratified fine- to coarse-grained pebbly sandstone, poorly-sorted, containing multidirectional trough or planar cross-bedding with truncation surfaces.
- J. 6839 feet; coarse-grained pebbly sandstone overlain by very fine- to medium-grained sandstone, sharp irregular contact. Contact and bedding in the overlying sandstone are inclined 12° .
- K. 6849 feet; black charcoal and shale flakes interlaminated with fine-grained sandstone. Bedding in the coarse-grained sandstone above the discontinuous shale laminae is inclined $18-20^{\circ}$. Pebbly sandstone below is slightly inclined. Opposite inclination direction is probably due to the core slab orientation.
- L. 6852 feet; cross-stratified fine- to medium-grained sandstone, moderately-sorted, containing multidirectional trough or planar cross-bedding with a truncation surface.



(Blatt, et al., 1980). At flow depths of 1 meter, mean velocities of 40 to 100 cm/sec are required to transport the maximum grain sizes of 2 to 13 mm observed in the L2 core (Hjulstrom, 1935). Some of the imbricated gravel beds appear inclined 16-21°. However, these beds contain more sand than the others and may be pebbly sandstone which is cross-stratified, and not inclined imbrication. Contacts between the conglomerate facies and the mudstone and shale facies are usually sharp. The contact between the conglomerate facies and the sandstone facies can be sharp, with the contact established by wavy, irregular shale lamination. However, the contact is usually gradational and the result of reverse or normal grading. Internal contacts between the structureless gravel beds and imbricated gravel beds are gradual.

Sandstone is the most prominent facies in the vertical sequence of the L2 core, and the section contains the most recognizable sedimentary structures: cross-stratification, parallel lamination, massive pebbly sandstone, and deformation features. Pebbles are scattered randomly throughout much of this facies. The stratified sandstone beds contain both low- and high-angle, multidirectional cross-bedding with bed set thicknesses ranging from 2 to 14 feet (0.6 to 4.3 m). Low angle stratification is inclined 5-8° (Figure 6-L), and high angle stratification is inclined 18-20° (Figure 6A). Multidirectional cross-stratification is observed at several intervals (Figure 6-F, H, and L), and was probably formed by current-transported sediment deposited in bars containing planar and/or trough cross-bedding. Parallel laminated sandstone occurs in 3-5 feet

(0.91-1.5 m) thick strata interbedded with the gravel beds, and cross-stratified sandstone beds. Grading is not apparent in the horizontally stratified sandstones. However, lamination is observed in 1 to 2 inch (2.5 to 5.0 cm) bands of alternating grain size (Figure 6-C). Pebbles as large as 25 mm are found in medium to coarse-grained sandstones (Figure 7-B). These sandstones which contain large pebbles appear to lack fabric (Figure 6-A and Figure 7-B). As for the structureless gravel beds in the conglomerate facies, this is probably due to rapid deposition (Blatt, et al., 1980). Soft sediment deformation features are mostly observed in the mudstones. However, small displacements on syndimentary faults also occur in the fine-grained sandstones (Figure 7-J). Contacts between the sandstone facies and mudstone facies are usually sharp (Figure 7-C, H, K, L, and 8-E).

The mudstone facies contains a substantial amount of silt and fine-grained sandstone. Fine-grained sand lenses may be starved ripples (Figure 7-E and K), and fine- to medium-grained sand lenses may also be starved ripples (Figure 8-A). Soft sediment deformation is pervasive in the mudstones (Figure 7-D, E, and L). Displacements on syndimentary faults are small, probably 1 to 5 inches (2.5 to 12.7 cm), but difficult to measure on the face of a slabbed core. Rapid current deposition is suggested by fluid escape structures observed in the S27 core (Figure 8-D). There is little evidence of bioturbation in the sediment throughout the vertical sequence. However, a few trace fossils were observed (Figure 8-D). Contacts with other sedimentary facies are sharp.

Figure 7. Sedimentary structures in vertical sequence of the Canyon granite wash conglomerate in the Parker Creek 1 (S27) core. The boldface letters in the lower left corner of the photographs refer to the captions below.

- A. 7032 feet; structureless gravel, poorly-sorted, well-cemented, pebble at base of photo is 54 mm in long axis diameter.
- B. 7033 feet; massive pebbly sandstone, poorly-sorted, pebble in upper slab is 28 mm in long axis diameter. Wavy lineation in the upper part of the photo is a crack in the slab, not a lamination.
- C. 7036 feet; silty mudstone overlain by fine- to coarse-grained sandstone, sharp even contact. Sandstone is inclined 8 to 10°.
- D. 7038 feet; silty mudstone with convoluted laminations overlies cross-stratified fine- to medium-grained sandstone, sandstone contains multi-directional trough or planar cross-bedding with a truncation surface in lower right corner of photo.
- E. 7040 feet; silty mudstone with fine-grained sandstone laminae, sandstone is probably starved ripple laminae, syndimentary fault with 20-40 mm displacement.
- F. 7041 feet; silty mudstone with suspended coarse-grained sand and pebbles.
- G. 7043 feet; silty mudstone overlain by fine- to coarse-grained sandstone, sandstone is poorly-sorted and grades upward into silty mudstone, sharp contact. A coarse-grained mass is suspended in the upper mudstone.
- H. 7044 feet; silty mudstone with fine- to medium-grained sand lenses overlain by medium- to coarse-grained sandstone. Sharp contact.
- J. 7074 feet; massive fine-grained sandstone with rock fragments displaced by syndimentary fault with unknown displacement.
- K. 7075 feet; silty mudstone with fine-grained sand lenses. Lenses are discontinuous, wavy, uneven, laminations. Medium- to coarse-grained sandstone overlies mudstone, sharp irregular contact.
- L. 7075.5 feet; pebbles and coarse-grained sandstone suspended in silty mudstone, 8 mm displacement on syndimentary fault in upper portion of photo.
- M. 7075.7 feet; silty mudstone with suspended fine- to medium-grained sand. Shale clast is 32 mm long and 12 mm thick and is also suspended in the mudstone.

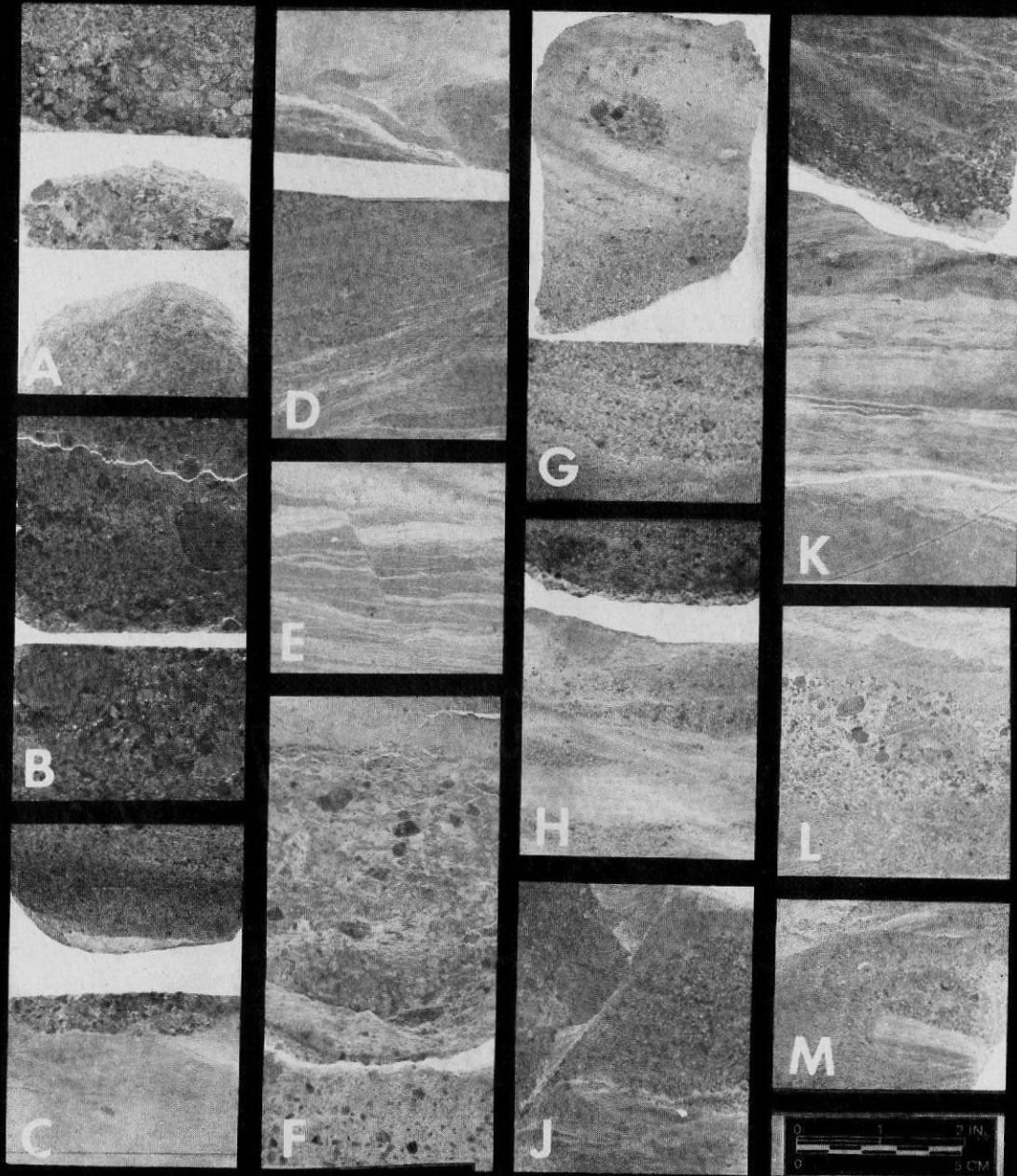
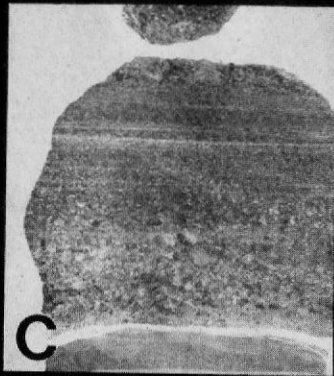
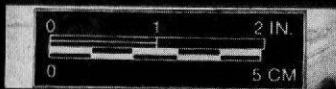
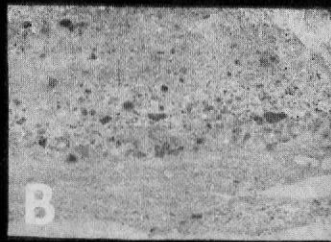


Figure 8. Sedimentary structures in vertical sequence continued from Figure 7, Parker Creek 1 (S27) core. The boldface letters in lower left corner of the photographs refer to the captions below.

- A. 7079 feet; silty mudstone with fine-grained sand. Sand laminae are wavy, uneven, and discontinuous, may be starved rippled laminae. Medium-grained sand lenses interbedded with mudstone in upper portion of photo.
- B. 7080 feet; medium-grained sandstone overlies fine-grained sandstone, which overlies silty mudstone. The mudstone and fine-grained sandstone are separated by a sharp contact.
- C. 7084 feet; coarse-grained sandstone grades upward into fine-grained sandstone with even, parallel, horizontal, continuous laminae. At very top of photo, faint contact is observed with coarse-grained sandstone repeated above.
- D. 7085 feet; silty mudstone with very fine-grained sand with convoluted laminae, may be a fluid-escape structure. Burrow at top left of photo.
- E. 7087 feet; very fine-grained sandstone abruptly overlies black shale with sharp contact.



Trace fossils present in the black shales and silty mudstones of the Parker Creek 1 (S27) core include Asterosoma, Chondrites, mini-Gyrolithes(?), Ophiomorpha(?), Planolites(?), and Teichichnus. In the Jay Taylor B-1 (L2) core the only trace fossil observed is Chondrites. The known distribution of the trace fossil types seen in the granite wash cores range from lagoonal to abyssal plain; the only environment common to these fossil types is the near shore, shelf environment (Chamberlain, 1978; Locke, 1983). Other fossils observed in the L2 core were broken and fragmented crinoid stems suspended in silty mudstone (Figure 6-E).

Composition

The conglomerate and sandstone compositions throughout the cored sequence are variable. Since the compositional percentages are influenced by the grain size, gravel size grains (> 2 mm) are analyzed separately from sand grains (< 2 mm) (Appendix III-A and III-B). The analyses show that the gravel population has a majority of granitic rock fragments, the sand population a majority of feldspars, and the very fine-grained sand and coarse-silt a majority of quartz. Average detrital compositions are summarized in Table 4.

The compositions from the L2 and S27 core samples plot within the arkose field (Folk, 1980). High granitic rock fragment and feldspar content characterize arkoses. The L2 core has an average of 68% granitic rock fragments plus feldspar and the S27 core has an average of 60%. The logarithmic rock fragment-to-feldspar ratio plot of the samples from the two cores shows that as grain size

Table 4. Average compositional and textural properties of the Canyon granite wash from the Jay Taylor B-1 (L2) and the Parker Creek 1 (S27) cores, Oldham County, Texas.

Well	Grain Size ^a			Detrital Composition ^b										Porosity % of total
	Mean mm	Max mm	σ mm	Gravel (> 2 mm)				Sand (< 2 mm)				Cement ^c CO ₃ % of total		
				Qz	F	Rx	Oth	Qz	F	Rx	Oth		Mx	
JTB1 (L2)	1.5	6.0	0.44-2.5	3	8	13	0	18	37	10	3	8	4	9
PC1 (S27)	0.83	4.2	.05-2.3	1	3	9	0	24	41	7	2	13	6	3.8

^aLong-axis measurements; σ = standard deviation

^bQz = monocrystalline quartz, F = feldspar, Rx = rock fragments including polycrystalline quartz, Oth = other detrital grains,

Mx = matrix (clays and chlorite).

^cCO₃ = carbonate cement.

increases, the rock fragment-to-feldspar ratio also increases (Figure 9) (Appendix IV). Since many of the larger gravel grains were excluded from the thin section analyses, the actual rock fragment-to-feldspar ratio is greater for some samples than the percentages calculated from the petrology.

Monocrystalline quartz content in the L2 core varies little and averages 21% (Figure 10). Composition of the very fine-grained sand and coarse-silt in the S27 core is primarily quartz, and therefore the core has an overall higher quartz content, averaging 25% (Figure 11), than the L2 core, which lacks fine-grained sediment. Monocrystalline quartz was recognized as having simple or wavy extinction, no cleavage, and a uniaxial interference figure.

Feldspar composition is primarily potassium feldspar, which is the host for the perthitic grains. The sands have very minor percentages of plagioclase. Potassium feldspar was identified by its gray to yellow interference colors, biaxial interference figure, and alteration features.

Rock fragments are primarily igneous rock fragments, but include small percentages of sedimentary rock fragments and polycrystalline quartz. Igneous rock fragments were recognized by the presence of quartz and feldspar combined in one grain. Most of the sedimentary rock fragments are clay clasts which are compressed between other grains.

Accessory minerals include muscovite, biotite, and zircon. Zircon was identified by its very high relief, and third or fourth-order interference colors. Oxides include anatase (Figure

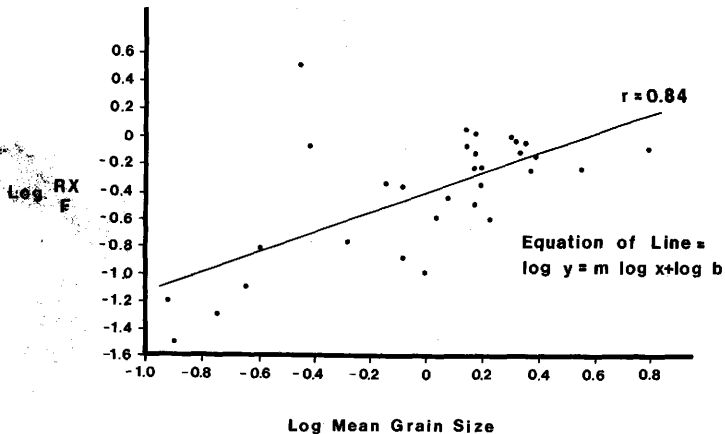
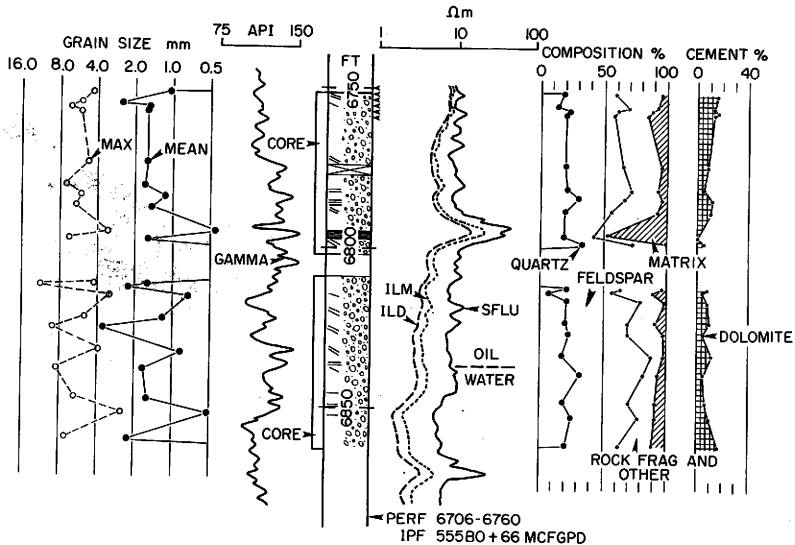


Figure 9. Logarithm of rock fragment (Rx)-to-feldspar (F) ratio versus logarithm of mean grain size. Least squares regression line has a correlation coefficient (r) of 0.84. Data is tabulated in Appendix IV.

Figure 10. Maximum and mean grain size and generalized composition plotted with gamma-ray and resistivity logs. Center lithology column shows the vertical sequence of the Canyon granite wash in the Jay Taylor B-1 (L2) core.

JAY TAYLOR B-1 (L2)



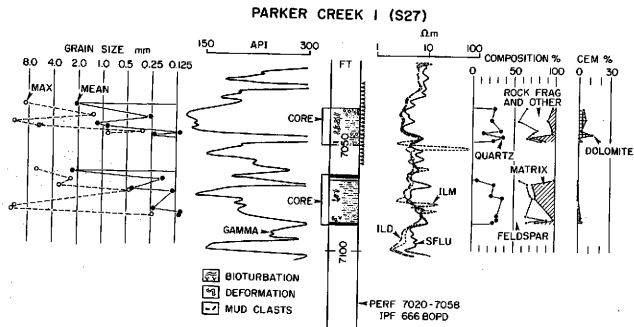


Figure 11. Maximum and mean grain size and generalized composition plotted with gamma-ray and resistivity logs. Center lithology column shows the vertical sequence of the Canyon granite wash in the Parker Creek I (S27) core.

12-G) and possibly also hematite or magnetite (Figure 12-C and 12-A). The oxides were opaque and recognized by reflected light.

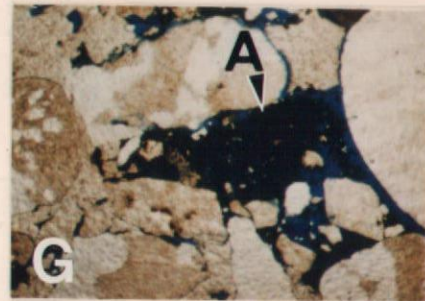
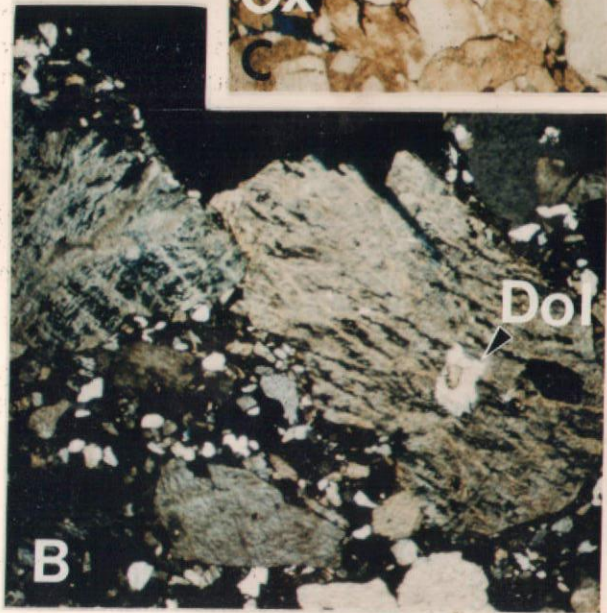
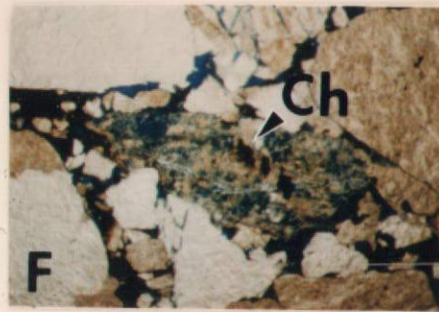
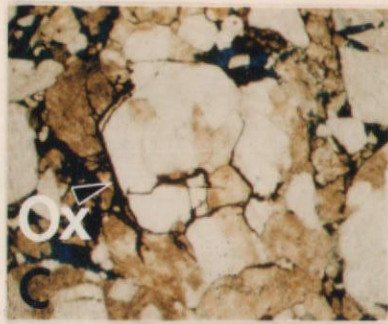
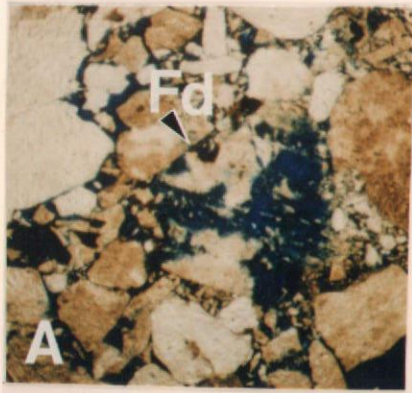
The matrix content of the conglomerate and coarse-grained sandstone beds is very low, averaging 8% and 13% in the L2 and S27 cores, respectively. However, it can range as high as 29% in the finer-grained sandstones. The matrix is the result of both detrital and authigenic processes. Detrital matrix is minor and is primarily the result of contemporaneous deposition of clay with the silt and sand. Authigenic matrix is mainly due to the alteration of feldspars to chlorite. The chlorite is green, yellow, and brown in plain polarized light, and occurs as fibrous and blocky particles. Some feldspars are almost completely obscured by chlorite alteration, and sericitization (Figure 12-F). Sericitization of the feldspar grain produces a dirty appearance in thin section, and renders the feldspars easily distinguishable from quartz grains.

Evidence of feldspar dissolution is common (Figure 12-A, B, D, and E). However, original pore space is much more abundant than dissolved pore space. Dissolution may have been caused by the migration of formation waters. The dissolution occurs randomly, and relatively unaltered grains exist in close proximity to dissolved grains (Figure 12-A, B, and F). Arkoses commonly contain feldspars in all stages of alteration (Blatt, et al., 1980).

Quartz overgrowths are only seen on a few very fine-grained sand particles. No overgrowths are observed on larger grains. The sand particles with quartz overgrowths were probably transported from another source area and did not form in place.

Figure 12. Photomicrographs of the Canyon granite wash conglomerate in the Jay Taylor B-1 (L2) core taken at 25x power. Blue color is epoxy and represents porosity. The bar scale represents 0.8 millimeter. The boldface letters in the lower left corner of the photographs refer to the caption below.

- A. 6751 feet; dissolved feldspar grain (Fd) in plain-polarized light, arrow indicates outline of the original grain. Opaque oxides may be hematite or magnetite. Some surrounding feldspar grains appear unaltered. Other feldspar grains are heavily sericitized, and appear dirty, brownish in color.
- B. 6784 feet; dissolved feldspars in cross-polarized light, dissolution occurs along selective plains of perthite. Dolomite rhombs (Dol) have replaced feldspar and have grown into the dissolved pore space. Surrounded feldspar grains appear unaltered, or sericitized.
- C. 6787 feet; opaque oxide (Ox) coats and penetrates grains along fractures. Other oxides are opaque rounded particles. The oxides may be hematite or magnetite.
- D. 6784 feet; dissolved feldspar in plain-polarized light. Feldspar grain is sericitized and partially dissolved. Corresponding photo E, in crossed-polarized light, shows dolomite rhombs that have replaced feldspar and have grown into dissolved pore space.
- E. 6784 feet; photomicrograph D in crossed-polarized light, dissolved feldspar grain, arrow indicates dolomite rhombs (Dol) replacing feldspar and growing into dissolved pore space.
- F. 6826 feet; dissolved feldspar in plain-polarized light, chlorite has replaced feldspar. Surrounding feldspar grains are unaltered or sericitized, but not dissolved.
- G. 6826 feet; opaque oxide, anatase (A), titanium oxide (TiO_2), forms in clusters in original and dissolved pore space. Surrounding feldspar grains are sericitized.
- H. Bar scale represents 0.8 millimeter.



Dolomite rhombs also replace feldspar grains. However, only small portions of the grains are replaced, and the rhombs seem to be found only in dissolved pore space (Figure 12-B, E). Chlorite also occurs as alterations of the dolomite rhombs.

Pyrite is seen in thin section with reflected light. It also occurs as nodules in the mudstones of the Parker Creek 1 (S27) core.

The amount of carbonate cement is low, averaging 4% in the L2 core and 6% in the S27 core. The cementation occurs in random patches. There is no evidence of silica cement. Fibrous dolomite cement is found between individual grains and in fractures in the pebbly sandstone and mudstone. Where cementation occurs, dissolution and chlorite alteration are apparently absent and grains are relatively unaltered. Oxides are also not present in these cemented zones. This suggests that cementation occurred before chlorite alteration. There is some evidence for several stages of cementation but the low cement percentage prevents a detailed analysis.

The Canyon granite wash characteristics suggest a relatively shallow and uncomplicated diagenetic history. The following mineralogical relationships recognized by Blatt et al, (1980) support this statement, 1) no formation of quartz overgrowths, 2) sericitization of K-feldspars, 3) dissolution of feldspars, and 4) precipitation of cement into pores. Other relationships which characterize deep burial such as pressure solution were not seen in the two cores.

Texture

The textural characteristics of the Canyon granite wash are highly variable (Figures 10, 11). The sediment is classified as immature (Folk, 1980). The L2 and S27 cores exhibit bimodal grain size distributions with a population of gravel, and a population of coarse to very-fine grained sand. Mean quartz sizes range from medium-grained sand to gravel in the L2 core and very-fine grained sand to gravel in the S27 core. The sediment is generally very poorly-sorted. Gravel and very-coarse grained sand are mostly angular in shape. Individual beds that coarsen upward, fine upward, and appear ungraded are present in both cores. This is probably the result of large fluctuations in discharge and other flow characteristics. The cores exhibit abrupt vertical and lateral changes in sorting and maximum and mean grain size.

The Canyon granite wash from the L2 core has average mean and maximum grain sizes of 1.5 mm and 6.0 mm, respectively (Table 4). The standard deviation ranges from 0.44 phi (well-sorted) to 2.6 phi (very poorly-sorted). The granite wash from the S27 core is finer grained, with average mean grain size of 0.83 mm and average maximum grain size of 4.2 mm. However, the long-axis measurement of the largest pebble observed in the core is 54 mm (Figure 7-B). The standard deviation ranges from .05 phi (very well-sorted) to 2.3 phi (very poorly-sorted).

The variability of grain size and composition suggests that the sediment was derived from a nearby source. The presence of fluid-escape structures, syndepositional faulting, and debris flow

deposits probably indicates rapid deposition and burial.

INTERPRETATION

Introduction

The Canyon granite wash conglomerate and sandstone consists of coarse-grained debris eroded from the Bravo Dome. The sediment was current transported across a carbonate shelf and deposited into the Oldham trough. The association of sedimentary structures, compositions and textures suggests short transport distance from a high-relief source area and is interpreted to be the result of fan-delta deposition. A fan-delta is an alluvial fan that progrades into a standing body of water from an adjacent highland (McGowen, 1970; Westcott and Ethridge, 1980). Imbricated gravel and cross-stratified bed sets are dominant and probably represent braided stream deposits. During the transgression which followed Canyon granite wash sedimentation, carbonate mounds developed on high-relief structures and shale filled the Oldham trough, eventually covering the carbonate mounds.

Alluvial Fan Deposits

Alluvial fan deposits can be divided into three depositional facies: proximal, medial, and distal. Braided stream processes are primarily responsible for transporting and depositing the sediment. Mean particle size and surface slope decrease from the head to the toe of alluvial fans (Friedman and Sanders, 1978).

The proximal facies is located at the apex of the fan complex where slope angles are highest. It is characterized by debris flows,

pebble imbrication and lack of stratification features (Klein, 1982). The sediment is poorly-sorted and shows a broad range of particle size. Particle shape is angular. Debris flow deposits are supported by a muddy matrix, and most of the sands are grain supported. In humid regions, stream flow dominates with less debris and mud flows (Friedman and Sanders, 1978).

The medial facies is characterized by cross-stratification, pebble imbrication, parallel lamination, and debris flows. The cross-stratification is developed by longitudinal and transverse bars. The medial facies is better sorted than the proximal facies because of the increase in sand content, but is generally still poorly-sorted. The gravel clasts are imbricated and the interbedded sandstone is parallel laminated.

The distal facies is located at the toe of the fan, and has the lowest slope. The sands are better sorted than the medial fan. However, some sands may contain gravel. The facies is characterized by cut and fill cross-stratification, convoluted lamination, low-angle forset beds, rip-up clasts and concretions. Pebbles are imbricated in the gravelly sand. The toe of a fan that builds out into a lake or shallow sea may be unstable and yield to sediment slumping (Neilson, 1982).

A normal vertical sequence shows the proximal facies prograding over the medial facies, and the medial prograding over the distal facies. Coals can form on abandoned fan segments where sediment is deposited in a lake or marsh (Klein, 1982).

Sediment Source

The Canyon granite wash is separated laterally from the granitic basement rocks of the Bravo Dome by platform carbonates (Figure 4). The granite wash was most likely transported across the carbonate platform by stream channels. However, only one such channel has been discovered, in the Manarte Field which lies just west of the study area on the carbonate platform. The channels may be related to the underlying Precambrian basement structure. Basement block faulting probably controlled the positions of the channels. The channels would have preferentially flowed in the low areas, and more channels have probably not been found because the grabens have not been drilled.

Erosive channels of granite wash are found in several wells above the Canyon Limestone. This granite wash has been informally named here as the Manarte granite wash (Appendix V). These channels may have been the conduits for granite wash found farther out in the basin and may have supplied the sediment to alluvial fans recognized by Dutton (1980a).

Depositional Environment of the Canyon Granite Wash

The morphology of the Canyon granite wash interval was determined by constructing isopachous maps and cross sections. Cross section A-A' trends southwest-northeast and shows the characteristic geometry of alluvial fans (Figure 4). The Strawn and Canyon granite wash are lens-shaped bodies that thin both toward and away from the sediment source. This probably reflects the continued uplift of the

adjacent highland during fan sedimentation (Bull, 1972). The internal geometry of the Canyon granite wash is very complex and is probably due to alternating intervals of transgression and progradation during the uplift of the Bravo Dome. The Lambert 1, Hryhor, and Sundance field area consists of a complex network of braided stream deposits.

The interval of Canyon granite wash examined in the Jay Taylor B-1 (L2) well represents the medial facies of an alluvial fan. Sedimentary structures, composition, and texture indicate rapid deposition from a nearby source and rapid burial. The dominant sedimentary structures are low-angle cross-stratification of fine- to very coarse-grained gravelly sandstone beds. The gravel grains are imbricated and some of the interbedded sandstone beds are parallel laminated. Structureless gravel beds and debris-flow deposits are also present. The cross-stratified sandstones probably represent channel and longitudinal or transverse bar deposits. The interval is generally very poorly-sorted. However, some beds are better sorted. Syndepositional faults indicate unstable slopes which also suggests rapid deposition and burial.

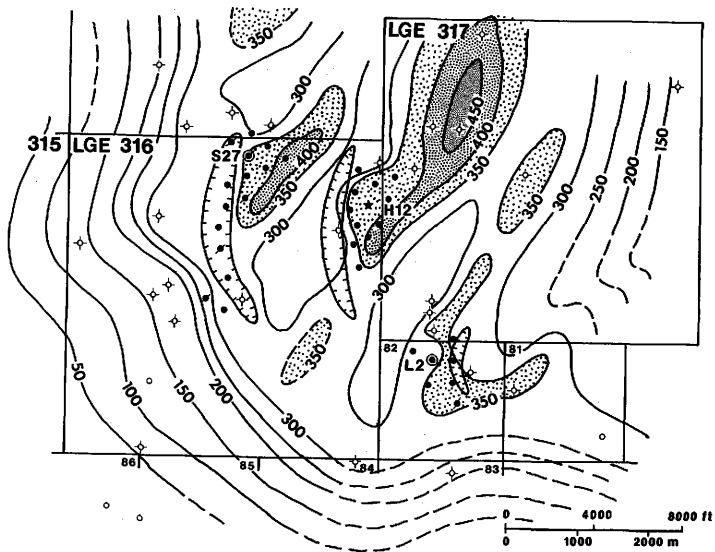
The Parker Creek 1 (S27) core represents the medial to distal fan facies. The core is dominated by marine mudstone. The most common sedimentary structures are convoluted lamination and other soft sediment deformation features. Conglomerate and sandstone beds are interbedded with the mudstone. These beds are primarily cross-stratified. This interval probably represents the transition between alluvial fan and marine sedimentation. The conglomerate and sandstone is better sorted than the L2 core but is generally

still poorly-sorted.

The sediment distribution of the Canyon granite wash in the Lambert 1, Hryhor, and Sundance field area illustrates the complex nature of this deposit (Figure 13). The highly variable gross thickness is probably due to two factors; 1) the complex sediment distribution of alluvial fan deposits, and 2) the complex structure of the area. Alluvial fan sediments consist primarily of braided stream deposits which diverge and overlap at random. This produces highly variable thicknesses of channel fill on a local scale. Nevertheless, the entire study area has a minimum thickness of at least 200 feet (61 m) of Canyon granite wash. The interval thickness in the Lambert 1 Field ranges from 236 to 378 feet (72 to 115 m); in the Hryhor Field from 237 to 497 feet (72 to 151 m); and in the Sundance Field from 288 to greater than 401 feet (88 to >122 m) (Appendix VI).

The gross isopachous map shows the position of the carbonate platform margin and Canyon granite wash lenses extending into the Odham Trough. The lenses reach a maximum thickness of 450 feet (137 m) and average 350 feet (106 m). The Canyon granite wash probably does not extend far to the east of the Ware Jupiter 1 (P70) well. Several wells have abnormal thicknesses due to faulting, and the hatched areas on the gross and net isopachous maps contain wells affected by faulting. These thicknesses were not used in constructing the isopachs. A section of the Canyon granite wash interval is repeated in the Aurora 11 (H22) well, Hryhor Field, by a high angle reverse fault. In the Lambert 1 Field, the Fulton King A-1 (L4) well is missing 125 feet of section because of a normal

Figure 13. Gross isopach of the Canyon granite wash interval in the Lambert 1, Hryhor, and Sundance fields showing the trend and morphology of the granite wash lenses. Hachured areas contain wells whose granite wash thickness is effected by faulting and therefore not used in mapping the trends. Contour interval is 50 feet.



fault.

The net isopachous map shows the same general features (Figure 14). Beds which have values on the gamma-ray log over 225 API units were counted as shale. Shale intervals range from 18 to 85 feet (5.5 to 26 m) in the Lambert 1 Field; 40 to 168 feet (12 to 51 m) in the Hryhor Field; and 28 to 93 feet (8.5 to 28 m) in the Sundance Field (Appendix VI). Most of the shale beds are found near the top of the granite wash section. The increase in marine shales toward the top of the section may be the result of transgression due to decreased subsidence and decreased sediment supply. The alternation of alluvial fan deposits and marine shale is probably the result of lateral shifting of braided stream channels, rather than basinwide sea-level fluctuations.

Canyon Limestone

The Canyon granite wash is closely associated with the Canyon Limestone that forms the carbonate platform across which granite wash was transported. This platform extends around the margins of the Palo Duro and Dalhart basins (Dutton, 1980a; Birsa, 1977), as well as the Oldham Trough. Maximum thickness of Canyon platform limestone is 712 feet (217 m) in the Amy 1 (P45) well (Figure 15). Here the Canyon Limestone rests directly on granitic basement.

In addition to forming platform areas, the Canyon Limestone also occurs as mound-like buildups on structural highs seaward of the platform edge. Carbonate mounds are thus closely associated with producing fields. The Lambert 1 and Hryhor fields are both

Figure 14. Net isopach of the Canyon granite wash interval in the Lambert 1, Hryhor, and Sundance fields showing the distribution of clean granite wash using a cutoff of 225 API units on the gamma-ray log. Hachured areas contain wells whose granite wash thickness is effected by faulting and therefore not used in mapping the trends. Contour interval is 50 feet.

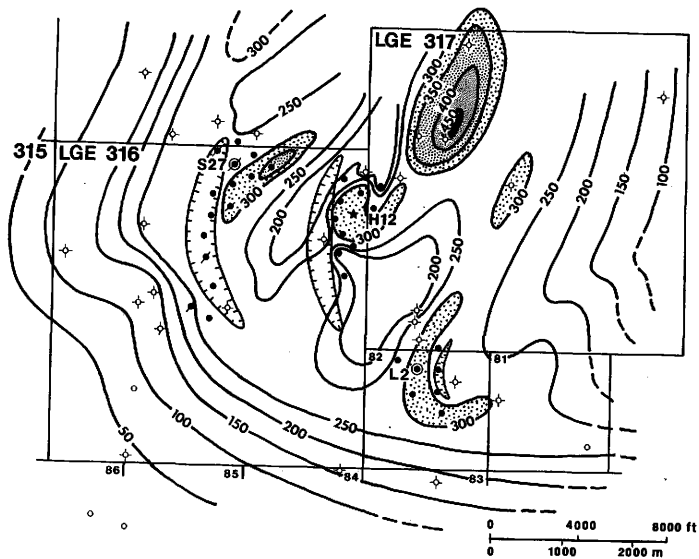
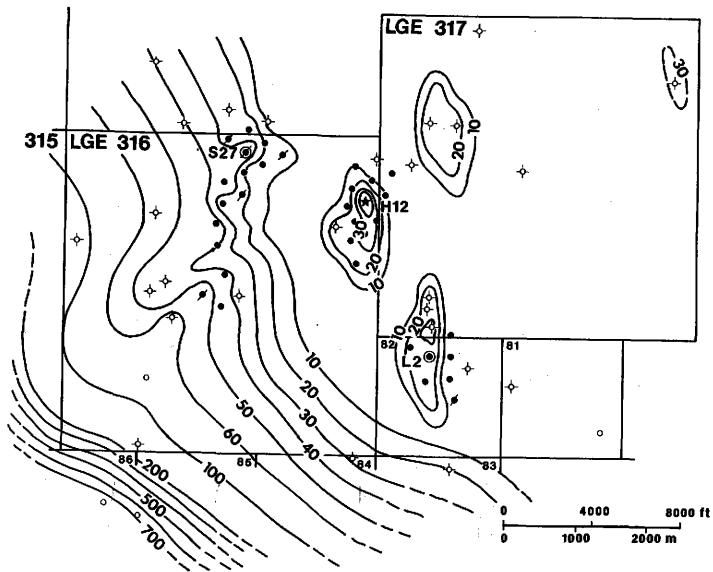


Figure 15. Isopach of the Canyon Limestone interval in the Lambert 1, Hryhor, and Sundance fields showing the carbonate platform margin. Mound-like buildups occur basinward of and along the margin. The carbonate mounds generally correlate with high relief structures, and therefore correlate with the fields. Contour interval is variable.



capped by carbonate buildups with maximum thicknesses of 38 feet (11.5 m) and 46 feet (14 m) respectively. The Sundance Field occurs on the platform margin but is associated with contour irregularities that may represent buildups along the edge of the platform.

Another carbonate buildup occurs in the Exotic 1 (P50) and New Atlantis (P59) wells. However, the Canyon granite wash is approximately 150 feet (46 m) structurally lower than in the Hryhor Field and does not produce in these wells (Figure 3).

The platform is shown to trend east-west near the Lambert 1 Field. However, it may continue to trend north-south, and the 20 feet (6 m) of carbonate buildup in the Mitchell Creek 1 (P58) well may represent another structural high.

The association of carbonate buildups with structural highs and productive reservoirs is potentially a very powerful tool for further exploration.

Structural Setting of the Fields

The study area is structurally complex, and the interpretation of seismic sections shows the presence of numerous faults. Most of the major faults are high-angle reverse faults, but a few normal faults also occur. In addition, an isolith was constructed on the interval thickness from the top of the Brown Dolomite to the top of the Canyon granite wash. The map showed abrupt changes in interval thickness which were explained by faulting. Major faults in the study area strike north-south and may curve slightly (Figure 3).

A typical seismic section shows two high-angle reverse faults which form the boundaries of the Hryhor and Sundance fields (Figure 16). The three fields in the study area occur on structural highs formed by high-angle reverse and normal faults. The Lambert 1 Field is structurally highest with maximum elevation of -3100 feet (-945 m). The Sundance Field has a maximum elevation of -3400 feet (-1037 m) and the Hryhor -3500 feet (-1067 m) (Figure 3).

Lambert 1 Field

The Lambert 1 Field is located on the up-thrown block of a normal fault. Compressional forces probably produced the two successive high-angle reverse faults which bound the Hryhor and Sundance fields. The normal faulting in the Lambert 1 Field is probably the result of extension produced when the Sundance block bent over. Other small faults are also thought to break the continuity of the field also.

Cross-section B-B' trends north-south and shows the variability in thickness through the field due to sedimentation and faulting (Figure 17). The Canyon granite wash interval thickens across the fault from 236 feet (72 m) in the Fulton King A-1 (L4) well to 373 feet (114 m) in the Fulton King A-6 (L9) well (Appendix VI). Increased thickness on the down-thrown side indicates movement of the fault during Middle Pennsylvanian deposition.

Lateral and vertical correlation is difficult due to the rapid shifting of the channels and bars. The fault cuts the Fulton King A-1 (L4) well at -3054 feet (-931 m) and shortens the section by

Figure 16. Migrated 12-fold seismic section showing the two high-angle reverse faults which form the boundaries of the Sundance and Hryhor fields. Several minor faults cut the section but only a few are indicated. Vertical scale is two-way travel time, measured in seconds. Line of the seismic line 4-123 is shown in Appendix II.

LINE 4-123

W

SUNDANCE FIELD

HRYHOR FIELD

E

◇
P68
SPRING
CREEK

●
S38
PARKER CREEK 12
(250' NORTH)

● ●
H14 H21
AURORA 3 AURORA 10
(200' SOUTH) (175' SOUTH)

A seismic reflection profile for Line 4-123, oriented West (W) to East (E). The vertical axis represents depth in feet, with markers at 0.5, 1.0, and 1.5. The geological layers are labeled on the left: BROWN DOLOMITE (top layer), CANYON LIMESTONE (middle layer), and PRECAMBRIAN GRANITE (bottom layer). The profile shows a complex structure with several faults and folds. Two faults are prominent, dipping towards the east. The Sundance Field is located in the center, and the Hryhor Field is located to the east. Well locations are marked with symbols: a diamond for P68 Spring Creek, a dot for S38 Parker Creek 12 (250' North), and two dots for H14 Aurora 3 (200' South) and H21 Aurora 10 (175' South).

63

Figure 17. Stratigraphic cross-section B-B' showing the vertical and lateral variation of the Canyon granite wash in the Lambert 1 Field. A normal fault cuts the Fulton King A-2 (L5) well. Datum is the top of the Strawn Limestone. Location of the cross-section is shown in Appendix II. No horizontal scale.

N

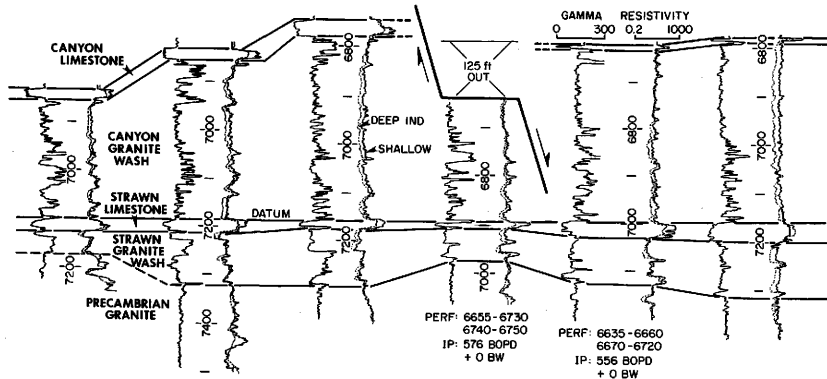
LAMBERT I FIELD

S

B



B'

L11
FULTON RANCHL8
FULTON KING A-5L10
FULTON KING A-7L4
FULTON KING A-1L5
FULTON KING A-2L9
FULTON KING A-6

approximately 125 feet (38 m). Restoration of the lost section results in a gross thickness of approximately 360 feet (110 m). This is in close accordance with the thickness predicted by the gross isopachous map, which was drawn excluding the Fulton King A-2 (L4) well (Figure 13).

The datum for cross-section B-B' is the Strawn Limestone. On the assumption that the Strawn Limestone was originally horizontal, the cross-section indicates that the surface of the Precambrian basement has 50 to 75 feet (15 to 23 m) of relief.

Hryhor Field

The Hryhor Field is located on the upthrown side of a high-angle reverse fault. Cross-section C-C' trends northwest-southeast and shows the high-angle reverse fault cutting the Aurora 12 (H23) well (Figure 18). The Canyon granite wash interval thickness is 333 feet (101 m) in the Aurora 6 (H17) well. The fault cuts the Aurora 12 (H23) well at -3909 feet (-1192 m) and approximately 175 feet (54 m) of the Canyon granite wash interval is repeated. The total interval thickness is 477 feet (145 m). Removal of the repeated section leaves a gross thickness of approximately 300 feet (90 m), which correlates well with the thicknesses of nearby wells not affected by faulting. The Aurora 2 (H13) may also be cut by the fault, repeating part of the Strawn granite wash interval.

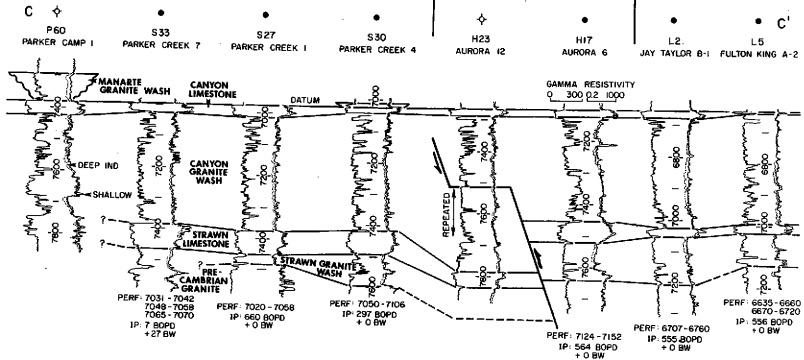
Figure 18. Stratigraphic cross-section C-C' showing the vertical and lateral variation of the Canyon granite wash across the study area. A high-angle reverse fault cuts the Aurora 12 (H23) well. The datum is the top of the Canyon Limestone. Location of the cross-section is shown in Appendix II. No horizontal scale.

NW

SUNDANCE FIELD

HRYHOR FIELD

LAMBERT I FIELD SE



Sundance Field

The Sundance Field also occurs on the upthrown side of a high angle reverse fault. Cross-section D-D' trends northwest-southeast (Figure 19). The datum is the Canyon Limestone. The fault bounding the west side of the Sundance Field is not evident on the cross-section but probably occurs between the Parker Camp 1 (P60) and Parker Creek 9 (S35) wells. The cross-section shows the eastward thickening of the Canyon granite wash interval. The fault between the Sundance and Hryhor fields may cut the Aurora 2 (H13) well, repeating part of the Strawn granite wash interval.

Depositional History

The granite wash sediments in the Oldham Trough form thick sequences of alluvial fan deposits basinward of the carbonate platform. Their position can be explained by a multiple sequence of transgressions and regressions during the Middle Pennsylvanian. A contributing factor to the depositional setting is the Bravo Dome, which was periodically active and supplied sediment to the adjacent basins.

The depositional sequence is illustrated by a diagrammatic cross-section which extends from the Bravo Dome to the Oldham Trough and represents a distance of approximately 40 miles (65 km) (Figure 20). Major depositional stages are numbered from 1 (oldest) to 6 (youngest).

During high stands of sea level, the carbonate platform built upward and outward. The Strawn Limestone platform prograded across

Figure 19. Stratigraphic cross-section D-D' showing the vertical and lateral variation of the Canyon granite wash in the Sundance field. A high-angle reverse fault cuts the section between the Parker Creek 11 (S37) and the Aurora 2 (H13) wells. The datum is the top of the Canyon Limestone. Location of the cross-section is shown in Appendix II. No horizontal scale.

NW

SUNDANCE FIELD

SE

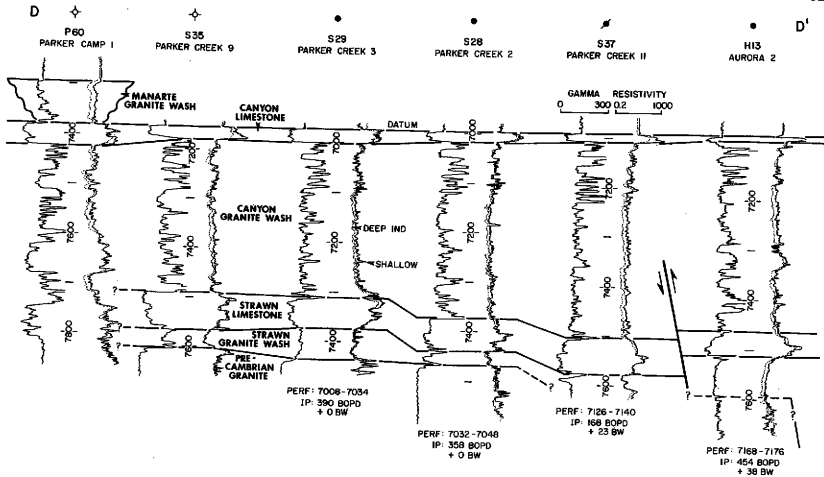


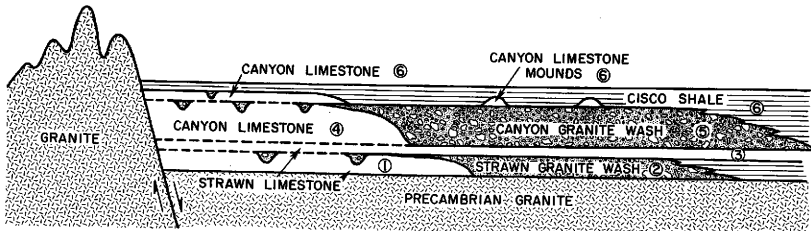
Figure 20. Diagrammatic cross-section from the Bravo Dome to the Oldham Trough showing the depositional history of the Canyon and Strawn sediments in the study area. The circled numbers represent six depositional stages during the Middle Pennsylvanian. The cross-section represents a distance of approximately 40 miles (65 km).

W

BRAVO DOME

E

OLDHAM TROUGH



SHALE

LIMESTONE

GRANITE WASH

GRANITE

GRANITE WASH CHANNELS

the uneven Precambrian granitic rocks (Stage 1). The cross-section, however, depicts the basement surface as horizontal for simplicity. Vertical uplift of the Bravo Dome provided a new source of coarse-clastic sediments which were carried across the platform and deposited as great fan-like sheets extending basinward from the platform slope (Stage 2).

A subsequent transgression allowed a second Strawn Limestone to buildup and back over the platform (Stage 3). This three stage sequence was repeated with a Canyon platform building up and out across the underlying Strawn Limestone (Stage 4). The Canyon Limestone probably did not prograde as far into the Oldham Trough as the Strawn Limestone because of continuing subsidence which may have increased water depths. Renewed uplift of the Bravo Dome provided new coarse-grained debris that was carried into the basin (Stage 5). The Canyon granite wash was then transgressed by a second Canyon Limestone and mound-like buildups formed on structural highs (Stage 6). The Canyon Limestone continued buildup of the carbonate platform and the trough was filled with shale.

This hypothesis requires great quantities of clastic sediment transported across the broad carbonate platform. There is evidence that the transport was through channels cut on the surface of the carbonate platform. One of these may have been preserved in the Manarte Field. The stream gradients were probably high enough to transport sediment entirely across the platform, leaving little evidence of channel fill. Also, the sediment that was left behind may have accumulated in low areas which have not been drilled.

Additional evidence for the channeling may exist in the variable thickness of the Canyon granite wash seen on the isopachous maps, but some thickness variation may be due to minor faulting. The entire area was a dynamic system with uplift and erosion of the Bravo Dome, subsidence of the basins, and small displacements on minor faults occurring simultaneously.

Finally, faulting died out during the Late Pennsylvanian as shown by the apparent decrease in the throw of the faults (Figure 16).

OIL ACCUMULATION

Oil Source

Source rocks for the Pennsylvanian oil are probably the black Cisco shales which lie directly over the Canyon Limestone and fill the adjacent Dalhart and Palo Duro basins. Based on geochemical evidence, Dutton (1980b) concluded that the Palo Duro Basin was not an area of major hydrocarbon generation. However, total organic carbon (TOC) data show that higher values are associated with Pennsylvanian and lower Permian basinal shales near the study area (Dutton, 1980b). Maximum TOC of 2.13% occurs at the Stanolind Herring 1 well which is 2000 feet (610 m) southeast of the Parker Camp 1 (P60) well. Clastic rocks that contain greater than 1.0% TOC are considered to be good source rocks (Tissot and Welte, 1978). In the Stanolind Herring 1 well, the kerogen color is orange and the vitrinite reflectance is 0.52% (Dutton et al., 1982). Basinal shales of the Pennsylvanian and Wolfcampian with relatively high values of TOC that coincide with abundant lipid-rich kerogen may have generated hydrocarbons. Thermal-maturity indicators studied by Dutton et al., (1982) show that source beds in the Palo Duro Basin have reached the threshold of the oil generation window.

Time and temperature are important in oil generation and destruction. A long exposure time for a source rock at low temperatures has the same effect as short exposure time at high temperatures. Waples (1980) applied N.V. Lopatin's method for timing of hydrocarbon generation to the burial history of the source rock. The burial

history of the Cisco shale in the study area is illustrated in a Lopatin diagram (Figure 21). A geothermal gradient of $1.0^{\circ}\text{F}/100$ feet ($18^{\circ}\text{C}/\text{km}$) was calculated from a bottom hole temperature of 149°F (65°C) in the Fulton Iris (P51) well at 8150 feet (2485 m). The geothermal gradient in the Palo Duro Basin is $1.1^{\circ}\text{F}/100$ feet ($20^{\circ}\text{C}/\text{km}$) (Dutton, 1980b).

Lopatin's method assumes that the relationship of maturity to time is linear, and therefore the relationship of maturity to temperature will be exponential (Waples, 1980). Time and temperature calculations were made from Figure 21 by estimating the time the Cisco shale spent in each temperature interval of 10°C (Table 5). The time was then multiplied by a temperature factor, defined by Lopatin, to obtain a time-temperature index (TTI). Total TTI was calculated by summing the TTI values for each interval.

Waples (1980) assigned total TTI values to different stages of hydrocarbon generation. A value of 15 total TTI marks the onset of oil generation. Peak oil generation correlates with 75 total TTI and 160 marks the end of oil generation. The upper limit for the occurrence of wet gas is about 1,500 total TTI.

The onset of oil generation in the Cisco shale occurred approximately 250 million years ago in the Late Permian, with oil being generated until the Late Triassic when the Cisco reached a depth in excess of 6000 feet (1830 m). Wet gas may also have been generated until the Late Cretaceous when burial was greater than 7000 feet (2134 m). Oil is produced in the Lambert 1, Hryhor, and Sundance fields. Gas is produced in the Hebe 1 (P53) well from the Canyon

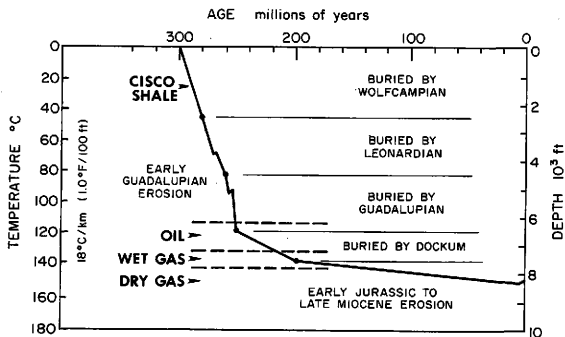


Figure 21. Lopatin diagram illustrating the burial history of the Cisco Shale and its relation to hydrocarbon generation, Oldham Trough, Northern Palo Duro basin. Format after Waples (1980).

Table 5. Calculation of time-temperature index (TTI) for burial history of the Cisco Shale in Figure 21.

Temperature Interval	Temperature Factor	Time (m.y.)	Interval TTI	Total TTI
20-30°C	2 ⁻⁸	6	0.02	0.02
30-40	2 ⁻⁷	5	0.04	0.06
40-50	2 ⁻⁶	5	0.02	0.08
50-60	2 ⁻⁵	5	0.16	0.25
60-70	2 ⁻⁴	8	0.50	0.75
70-80	2 ⁻³	6	0.75	1.5
80-90	2 ⁻²	3	0.75	2.2
90-100	2 ⁻¹	14	7.0	9.2
100-110	1	3	3.0	12.2
110-120	2	11	22.0	34.2
120-130	4	25	100.0	134.2
130-140	8	88	704.0	838.2
140-150	16	128	2048.0	2886.2

granite wash, and the Rodger 1 well, 3 miles (5 km) north of the study area, has produced gas also.

Oil could have been generated earlier in the equivalent shales deeper in the Dalhart and Palo Duro basins. However, Dutton's (1980b) geochemical data suggest that these shales may not have had TOC values, kerogen compositions, and vitrinite reflectances sufficient for hydrocarbon generation.

Trapping Mechanisms

The Cisco shales probably generated the oil produced from the Lambert 1, Hryhor, and Sundance fields. A deep down-dropped fault block that trends east-west is located approximately 1 mile (1.6 km) north of the study area. It contains shale that is buried about 1600 feet (488 m) deeper than the Cisco shale in the study area. This fault may have provided a migration route along with other minor faults for the oil found in the granite wash reservoirs.

The oil migrated into structurally high areas produced by faulting, and the faults prevented further migration. The Sundance Field is bounded by a high-angle reverse fault. The Parker Creek 9 (S35), Spring Creek (P68), Connie (P47), and the Single Fold (P66) are located on the down-dropped block and do not produce.

The Hryhor Field is also bounded by a high-angle reverse fault. The Aurora 12 (H23) is located on the down-dropped block and does not produce. The Lambert 1 and the Hryhor fields are separated by a structural low (Figure 3). The Lambert 1 is approximately 400 feet (122 m) structurally higher than the Hryhor field and

produces from the upthrown block of a normal fault. It is possible that before movement on the normal fault began, the Hryhor and Lambert 1 field were a single continuous reservoir. Subsequent deformation may have produced the trough that now separates the fields.

Log Interpretation

Determination of porosity from well logs is dependent upon assumed values for matrix density and fluid density. Analyses of the L2 and S27 cores provide the opportunity to compare porosity values measured from the cores with those calculated from Formation Density Logs. Core porosity values generally approximate true porosity and in any case are likely to represent maximum values.

Average porosities and permeabilities measured for stratigraphic intervals from the L2 and S27 cores are presented in Table 6. The intervals correspond to those described in Appendix III. Porosity values range from 3 to 16.7 percent. Permeability ranges from 0.1 to 613 md. Porosity and permeability are highest in gravelly sandstones and conglomerates.

Porosity and permeability values for the L2 core are presented in graphic form in Figure 22. Between 6800 and 6750 feet (2073 and 2058 m) porosity and permeability generally increase upward. Below 6800 feet, they are variable and show no discernable pattern. Oil saturation decreases from about 10% at the top of the core to 0% at the bottom. Water saturation shows a corresponding downward increase from about 50% to 90%.

Table 6. Average porosities and permeabilities for the Canyon granite wash, Lambert 1 and Sundance fields, Oldham County, Texas. Interval footage correlates with core descriptions (Appendix III).

Well	Interval (ft)	Footage (ft)	Number of Samples	Porosity		Permeability	
				Mean (%)	Range (%)	Geometric Mean (md)	Range (md)
L2	6751-6765	14	14	13.5	8.2-16.1	91	18-613
	6765-6770	5	5	11	8.8-13	18.5	4.6-34
	6770-6774	4	4	13	12-13.8	25	15-37
	6774-6777	3	3	13	11.8-13.9	16	13-26
	6777-6788	11	11	12	8.6-14.1	15	5.8-65
	6788-6794	6	6	9	3.5-12.6	3	0.2-13
	6794-6796	2	shale				
	6796-6799	3	3	6	3-9	0.6	0.1-1.6
	6799-6802	3	3	12.3	9.9-15.7	24	5.6-112
	6802-6809	7	core missing				
	6809-6812	3	3	14.5	13.8-15.2	23	22-24
	6812-6814	2	2	10.6	8.7-12.5	3.5	1-12
	6814-6816.5	2.5	3	12.3	6.8-15.6	14	4.4-26
	6816.5-6822	5.5	5	13.5	11.4-15.6	27.5	17-53
	6822-6833	11	11	13.3	8.9-16	26.5	8-290
	6833-6839.5	6.5	7	12.2	4-15.9	9	5.1-15
	6839.5-6852	12.5	12	12.5	4.6-16.1	7	0.6-23
6852-6862	10	10	15.3	14.7-16.7	36	11-123	
S27	7032-7036	4	4	12	10.9-13.1	22	13-34
	7036-7038	2	shale				
	7038-7039	1	1	9.4	-	0.3	-
	7039-7042	3	shale				
	7042-7043	1	1	10.2	-	<0.1	-
	7043-7044	1	1	15.2	-	0.4	-
	7044-7050	6	shale				
	7050-7064	14	core missing				
	7064-7065.5	1.5	shale				
	7065.5-7066	.5	1	8.0	-	0.2	-
	7066-7073	7	shale				
	7073-7074	1	1	10.1	-	2.9	-
	7074-7076	2	shale				
	7076-7088	12	4	6	4.8-6.7	0.2	0.1-0.3

md = Millidarcy

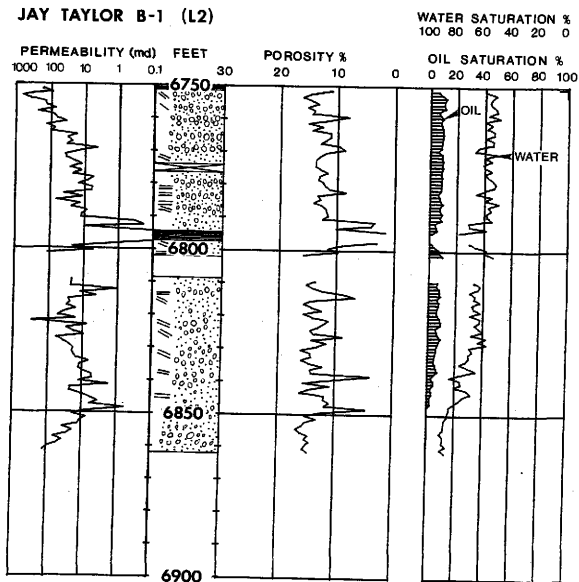


Figure 22. Core analysis showing porosity, permeability and fluid saturations in the Canyon granite wash interval, Jay Taylor B-1 (L2), Lambert 1 Field.

Porosities calculated from density logs are consistently higher than core analysis porosities. A cross plot of bulk density and porosity values from both core analyses and density logs illustrates the higher log porosities, which are represented by solid squares on Figure 23. The distribution of core porosities indicates a matrix density value of about 2.60 gm/cm^3 for the granite wash. This contrasts with the matrix density value of 2.71 gm/cm^3 used in density log porosity calculations. If matrix density is calculated theoretically based on the average mineralogical composition as determined in thin-section, the resulting value is approximately 2.59 gm/cm^3 (Table 7). This suggests that the matrix density of 2.60 gm/cm^3 determined from Figure 23 is close to the actual value. In addition, grain densities from the granite wash intervals in the L2 core are also in the 2.59 to 2.64 gm/cm^3 range.

A cross plot of permeability and porosity from the Jay Taylor B-1 (L2) core shows an abrupt change in the relationship of these two values (Figure 24). This change occurs at a porosity value of 9.5% and a permeability value of 1.5 md.

Formation water resistivity was determined by a cross plot method used to interpret well log data (Pickett, 1966). Resistivity and well log porosity are plotted on logarithmic scales. The plot for the Jay Taylor B-1 (L2) well indicates a water resistivity (R_w) of 0.025 ohm-meter (Figure 25). Water resistivity for the Fulton King A-2 (L5) well is 0.028 ohm-meter (Figure 26).

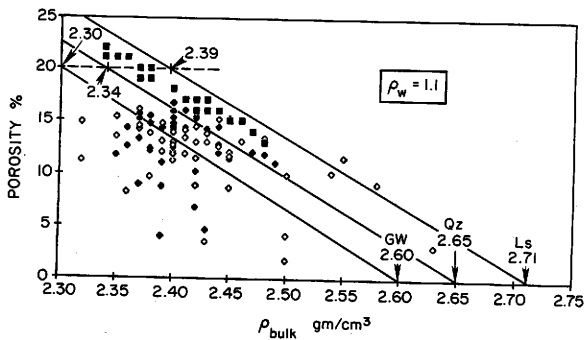


Figure 23. Cross plot of porosity and bulk density from the Jay Taylor B-1 (L2) showing estimated bulk density of the Canyon granite wash. Squares indicate log data, open and closed triangles indicate porosity data from the core analysis, and bulk density data from the density log.

Table 7. Calculation of Granite Wash bulk density.

Composition	Percentage	Density g/cm ³	Constituent Density g/cm ³
Quartz	20	2.65	0.53
Orthoclase	45	2.56	1.152
Rock Fragments	25	2.60	0.65
Matrix	<u>10</u>	2.55 ^a	<u>0.255</u>
Total	100%		2.59 g/cm ³

^aShale density from density log

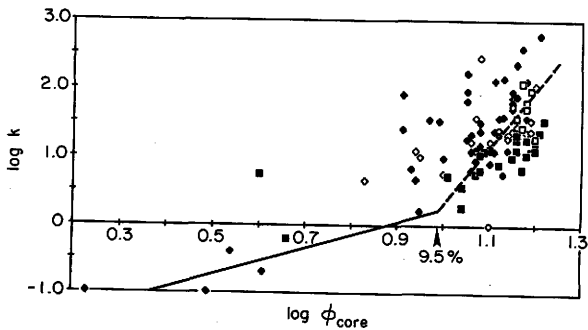


Figure 24. Cross plot of permeability and porosity from the Jay Taylor B-1 (L2) core (Figure 23) showing bimodal distribution of porosity. An apparent porosity cutoff is 9.5% and permeability cutoff is 1.5 md.

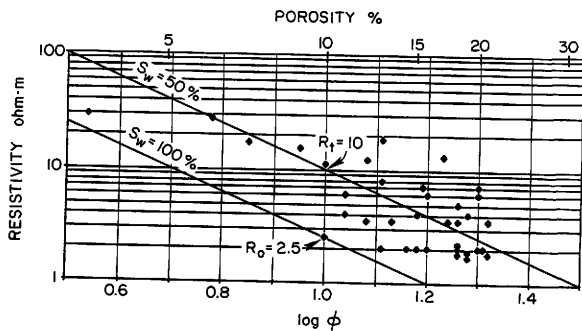


Figure 25. Pickett plot for Jay Taylor B-1 (L2) well showing water resistivity (R_w) of 0.025 ohm-m and variations in water saturation (S_w).

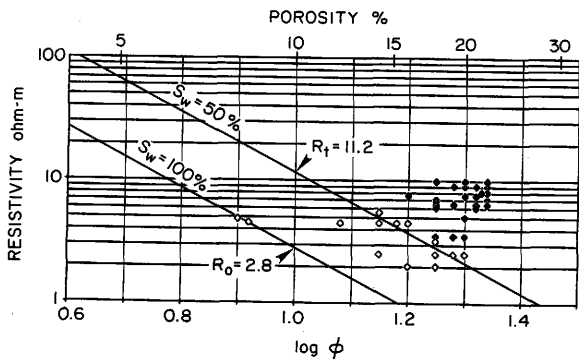


Figure 26. Pickett plot for Fulton King A-2 (L5) well showing water resistivity (R_w) of 0.028 ohm-m and variations in water saturation (S_w).

Minimum water resistivity values measured from drill stem tests range from 0.027 to 0.029 ohm-meter at 135°F bottom hole temperature. Based on these values, all perforated intervals which produced oil or oil and water lie above the line of 50% water saturation. From this plot it can be concluded that for water saturation calculations, the density log values for porosity are correct. The cementation exponent (m) is equal to 2 for log-derived values of porosity.

However, the log-derived porosities do not agree with core porosities (Figure 23). This means that for true porosities the cementation exponent has a value different from 2.

In summary, the log-derived values are satisfactory for calculation of water saturation, and for selection of zones for oil production. However, for economic evaluation of the reservoir, log-derived values of porosity should be corrected in order to calculate more realistic estimates of oil in place.

Reservoir Properties

Porosity and permeability data from the Jay Taylor B-1 (L2) and Parker Creek 1 (S27) core analyses were classified in an effort to describe the average properties of the reservoir, and evaluate porosity distributions, net pay sand, and permeability distributions. The data were classified into ranges of 1% porosity (Figures 27 and 28). The number of occurrences in a particular range is referred to as the frequency and expressed as a percentage. The cumulative frequency is the sum of the frequency percentages of each range. Most porosity distributions are relatively symmetrical (bell-shaped

Figure 27. Classification of porosity data into ranges of 1 per cent porosity for all samples from the Jay Taylor B-1 (L2) core. The data are shown on the: A) frequency histogram and cumulative frequency curve, and B) cumulative frequency curve plotted on an arithmetic probability scale.

<u>ϕ Ranges</u>	<u>No. of Samples</u>	<u>Frequency (%)</u>	<u>Cumulative Frequency (%)</u>
1-2	1	0.99	0.99
2-3	0	0.0	0.99
3-4	2	1.98	2.97
4-5	3	2.97	5.94
5-6	0	0.0	5.94
6-7	1	0.99	6.93
7-8	0	0.0	6.93
8-9	6	5.94	12.87
9-10	2	1.98	14.85
10-11	3	2.97	17.82
11-12	14	13.86	31.68
12-13	14	13.86	45.54
13-14	16	15.84	61.38
14-15	21	20.79	82.17
15-16	14	13.86	96.03
16-17	4	3.96	99.90

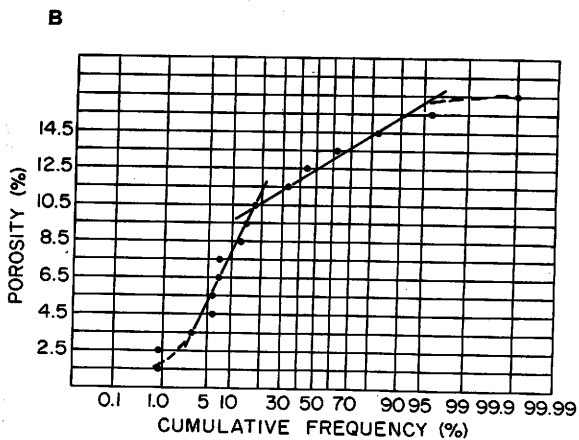
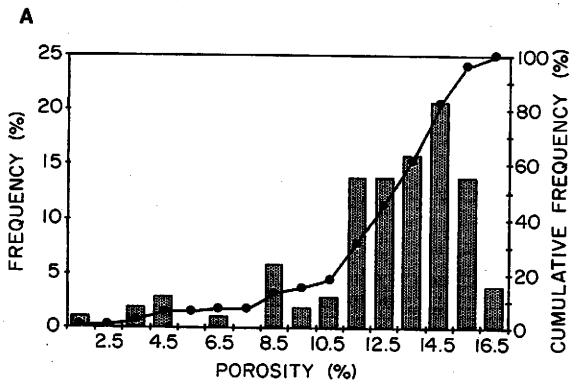
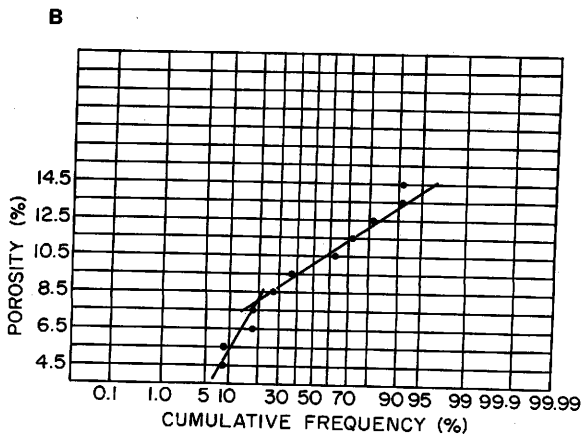
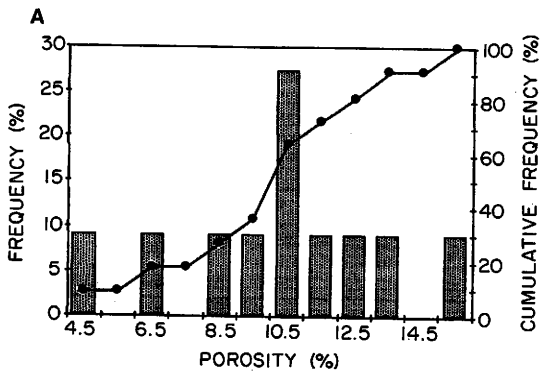


Figure 28. Classification of porosity data into ranges of 1 per cent porosity for all samples from the Parker Creek 1 (S27) core. The data are shown on the; A) frequency histogram and cumulative frequency curve, and B) cumulative frequency curve plotted on an arithmetic probability scale.

<u>ϕ Ranges</u>	<u>No. of Samples</u>	<u>Frequency (%)</u>	<u>Cumulative Frequency (%)</u>
4-5	1	9.1	9.1
5-6	0	0.0	9.1
6-7	1	9.1	18.2
7-8	0	0.0	18.2
8-9	1	9.1	27.3
9-10	1	9.1	36.4
10-11	3	27.3	63.6
11-12	1	9.1	72.7
12-13	1	9.1	81.8
13-14	1	9.1	90.9
14-15	0	0.0	90.9
15-16	1	9.1	99.9



curve) (Amyx et al., 1960). However, the L2 core data do not produce a normal distribution (Figure 27a). One possible reason for this deviation is that leached feldspars may have produced enough secondary porosity to skew the distribution.

Porosity ranges from 1 to 17% in the L2 core with a mean of 15% and a median of 12.8% (Figure 27a). The median is the value of the porosity corresponding to the 50% point on the cumulative frequency curve, and divides the histogram into equal parts (Amyx, et al., 1960). The bimodal distribution is easily recognized when the data are plotted on arithmetic probability paper. A normal distribution plotted on arithmetic probability paper approximates a straight line (Amyx et al., 1960). However, the L2 core data produce a segmented line which represents two porosity distributions (Figure 27b).

The S27 core has porosities ranging from 4 to 16% with a mean of 15% and a median of 10.2% (Figure 28a). The data produce a bimodal distribution. Less data were available, but thin section analysis indicated feldspar leaching similar to the L2 core. The data produce a segmented line when plotted on arithmetic probability paper (Figure 28b).

The cumulative volume capacity for the classified data of the L2 and S27 cores shows the net productive granite wash as determined by a porosity distribution (Figures 29 and 30). For the L2 core, Lambert 1 field, 97.5% of the storage capacity is represented by samples having porosities of 8.5% or greater. Therefore a cutoff value of 8.5% porosity used to determine net pay granite wash would

Figure 29. Calculation of porosity distribution from classified data for determination of cumulative capacity for the Jay Taylor B-1 (L2) core. The data are shown on a cumulative capacity curve.

ϕ Range	Mid-value of range, % ϕ_i	No. of Samples	Frequency Fraction F_i	Capacity	Fraction Capacity	Cumulative Capacity (%)
1-2	1.5	1	0.0099	0.0148	0.0012	99.8
2-3	2.5	0	0.0	0.0	0.0	99.7
3-4	3.5	20	0.0198	0.0693	0.0055	99.7
4-5	4.5	3	0.0297	0.1336	0.0106	99.1
5-6	5.5	0	0.0	0.0	0.0	98.1
6-7	6.5	1	0.0099	0.0643	0.0051	98.1
7-8	7.5	0	0.0	0.0	0.0	97.5
8-9	8.5	6	0.0594	0.5049	0.0401	97.5
9-10	9.5	2	0.0198	0.1881	0.0149	93.5
10-11	10.5	3	0.0297	0.3118	0.0247	92.1
11-12	11.5	14	0.1386	1.593	0.1266	89.6
12-13	12.5	14	0.1386	1.732	0.1376	77.0
13-14	13.5	16	0.1584	2.138	0.1699	63.1
14-15	14.5	21	0.2079	3.014	0.2390	46.1
15-16	15.5	14	0.1386	2.148	0.1707	22.3
16-17	16.5	4	0.0396	0.6534	0.0519	5.2

$$\text{Capacity} = \phi_i F_i$$

$$\text{Porosity average} = \phi_a = \frac{\sum \phi_i F_i}{\sum F_i} \quad \text{Fraction capacity} = \frac{\phi_i F_i}{\phi_a} \quad \text{Cumulative Capacity} = \sum_{i=1}^n \frac{\phi_i F_i}{\phi_a}$$

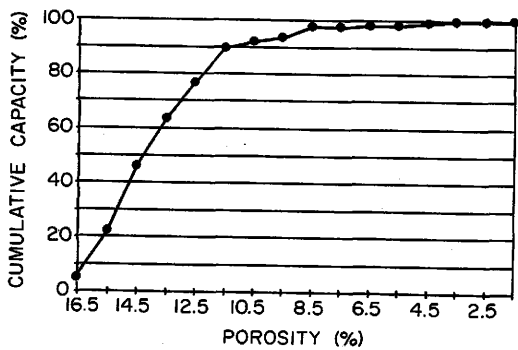


Figure 30. Calculation of porosity distribution from classified data for determination of cumulative capacity for the Parker Creek 1 (S27) core. The data are shown on a cumulative capacity curve.

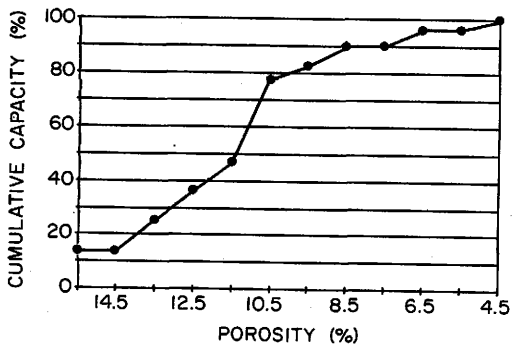
ϕ Range	Mid-value of range, $\% \phi_i$	No. of Samples	Frequency Fraction F_i	Capacity	Fraction Capacity	Cumulative Capacity (%)
4-5	4.5	1	0.0909	0.4091	0.0396	99.9
5-6	5.5	0	0.0	0.0	0.0	96.0
6-7	6.5	1	0.0909	0.5908	0.0573	96.0
7-8	7.5	0	0.0	0.0	0.0	90.3
8-9	8.5	1	0.0909	0.7726	0.0749	90.3
9-10	9.5	1	0.0909	0.8635	0.0837	82.8
10-11	10.5	3	0.2727	2.86	0.277	77.4
11-12	11.5	1	0.0909	1.045	0.1013	46.7
12-13	12.5	1	0.0909	1.136	0.1102	36.6
13-14	13.5	1	0.0909	1.227	0.1190	25.6
14-15	14.5	0	0.0	0.0	0.0	13.7
15-16	15.5	1	.0909	1.408	0.1365	13.7

$$\text{Capacity} = \phi_i F_i$$

$$\text{Porosity average} = \phi_a = \phi_i F_i$$

$$\text{Fraction capacity} = \frac{\phi_i F_i}{\phi_a}$$

$$\text{Cumulative Capacity} = \sum_{i=1}^n \frac{\phi_i F_i}{\phi_a}$$



include at least 97% of the producible hydrocarbons. Using a cutoff value of 9.5% porosity, as suggested in the previous section, would include more than 93.5 percent of the producible hydrocarbons.

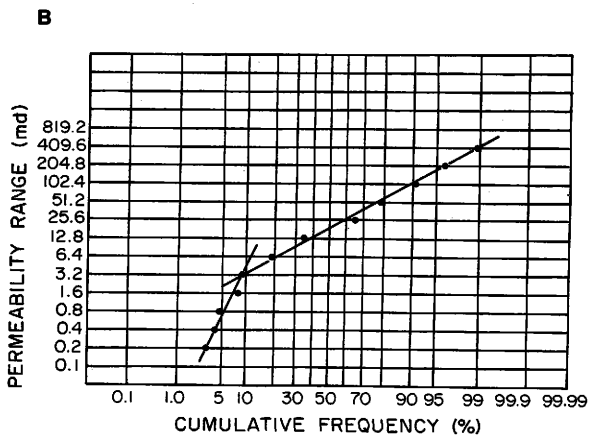
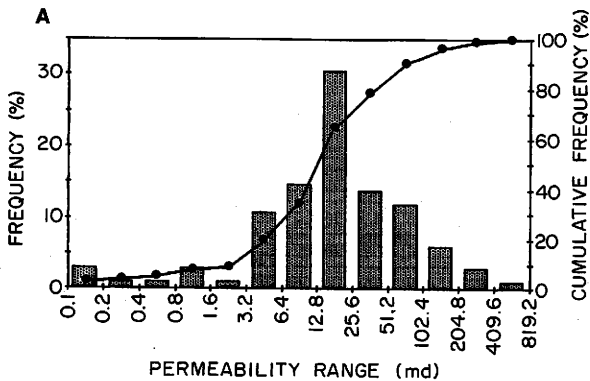
The storage capacity of the granite wash in the S27 core, Sundance field, is greater than the L2 core in the lower porosity ranges (Figure 30). A cutoff of 6.5% porosity includes only 96% of the producible hydrocarbons, and an 9.5% porosity cutoff value would include less than 90%.

Permeability data from the L2 core were also classified in order to estimate an average value (Figure 31). Data were analyzed in the same manner as the porosity data except in the selection of the ranges. The permeability ranges are selected on equal intervals of the logarithm of permeability (Amyx et al., 1960). Permeability ranges from 0.1 to 613 md with a mean of 17.5 md (Figure 31A). Since permeability is classified on a logarithmic scale the mean is calculated geometrically. The data are not normally distributed and, like the porosity distribution, are skewed. The data when plotted on arithmetic probability paper produce a segmented line (Figure 31B). This indicates that more than one normal distribution exists. The presence of two permeability distributions could be due to vertical variations in the granite wash beds or lateral variations. In this case they are probably vertical variations. As illustrated in Figure 22, the permeability decreases from 613 to an average of 20 md in the upper section of the core, possibly due to a subtle decrease in grain-size and/or increase in matrix content of the granite wash downward.

Figure 31. Classification of permeability data into equal logarithmic intervals. The data are shown on the; A) frequency histogram and cumulative frequency curve, and B) cumulative frequency curve plotted on an arithmetic probability scale.

Permeability Range	No. of Samples	Frequency (%)	Cumulative Frequency (%)
.1-.2	3	2.94	2.94
.2-.4	1	0.98	3.92
.4-.8	1	0.98	4.90
.8-1.6	3	2.94	7.84
1.6-3.2	1	0.98	8.82
3.2-6.4	11	10.78	19.60
6.4-12.8	15	14.70	34.30
12.8-25.6	31	30.39	64.69
25.6-51.2	14	13.72	78.41
51.2-102.4	12	11.76	90.17
102.4-204.8	6	5.88	96.05
204.8-409.6	3	2.94	98.99
409.6-819.2	1	0.98	99.97

Ranges calculated by: $j = \log_2 \frac{k_j}{k_1} = k_j = 2^j k_1$ where $j = 1, 2, 3 \dots$
 k_j = range limits
 k_1 = initial permeability = .1 md



CONCLUSIONS

Canyon and Strawn granite wash conglomerates and sandstones were derived from granitic rocks of the Bravo Dome. Two carbonate platforms developed and prograded across the Precambrian basement. The granite wash was transported across the carbonate platforms by streams and deposited in the Oldham Trough in fan-deltas. The granite wash sediments are generally very poorly-sorted and are primarily composed of granitic rock fragments and feldspar. The sedimentary structures are dominately imbricated gravels and cross-stratified sandstones. The association of primary and secondary rock properties suggests rapid deposition and shallow burial history. The sandstones are concentrated in narrow channel-like bodies that extend northeastward across the area from the base of the carbonate platforms.

Six depositional stages for the Middle Pennsylvanian are recognized; 1) Strawn Limestone platform development and progradation, 2) Strawn granite wash progradation, 3) a second Strawn Limestone development due to transgression and basin subsidence, 4) Canyon Limestone platform development and progradation, 5) Canyon granite wash progradation, and 6) a second Canyon Limestone development due to transgression and basin subsidence, with mound-like buildups occurring on structural highs, and shale filling the Oldham Trough.

The Cisco shales of the Middle and Late Pennsylvanian are the probable source rocks for the Pennsylvanian oil. Temperatures and burial depth were great enough for the shales to generate oil and possibly wet gas. Oil accumulated in structural traps located on

upthrown blocks bounded by high-angle reverse and normal faults.

Interpretation of reservoir properties from well logs presents some problems. Grain density of the granite wash is approximately 2.60 gm/cm^3 , and porosities calculated at 2.71 gm/cm^3 (limestone density) produce values approximately 5% too high. Water resistivities of 0.028 ohm-meter are calculated from resistivity-porosity plots. Reasonable net pay cutoff values in these granite wash reservoirs are 9.5% for porosity and 1.5 md for permeability.

Future exploration for granite wash reservoirs should concentrate on finding structurally high areas located along or slightly basinward of the carbonate margin which rims the Oldham Trough and the Dalhart and Palo Duro basins. The regional distribution of Pennsylvanian granite wash indicates that the channels cut across the platforms and produced fan-like sheets on the slopes of the platform and out into the basins.

REFERENCES CITED

- Adams, J.E., 1954, Mid-Paleozoic paleogeography of Central Texas, in Guidebook, Cambrian field trip-Llano area: San Angelo Geol. Soc., p. 70-73.
- Adler, F.J., W.M. Caplan, M.P. Carlson, E.D. Goebel, H.T. Henslee, I.C. Hicks, T.G. Larson, M.H. McCracken, M.C. Parker, B. Rascoe, Jr., M.W. Schramm, Jr., and J.S. Wells, 1971, Future petroleum provinces of the mid-continent, Region 7, in I.H. Cram, ed., Future petroleum provinces of the United States - Their geology and potential: AAPG Memoir 15, v. 2, p. 985-1120.
- American Petroleum Institute, American Gas Association, and Canadian Petroleum Association, 1980, Reserves of crude oil, natural gas liquids, and natural gas in the United States and Canada as of December 1979: API, AGA, and CPA, v. 34, p. 78.
- Amyx, J.W., D.M. Bass, Jr., and R.L. Whiting, 1960, Petroleum reservoir engineering-Physical properties: New York, McGraw-Hill Book Company, p. 536-559.
- Birsa, D.S., 1977, Subsurface geology of the Palo Duro Basin, Texas Panhandle: Master's thesis, University of Texas at Austin, Austin, Texas, 360 p.
- Blatt, H., G. Middleton, and R. Murray, 1980, Origin of sedimentary rocks: New Jersey, Prentice-Hall Inc., p. 121-123, 136, 631, 640.
- Budnik, R., and D. Smith, 1982, Regional stratigraphic framework of the Texas Panhandle, in T.C. Gustavson and others, eds., Geology and geohydrology of the Palo Duro Basin, Texas Panhandle, a report on the progress of nuclear waste isolation feasibility studies (1981): The University of Texas at Austin, Bureau of Economic Geology, Geological Circular 82-7, p. 38-86.
- Bull, W.B., 1972, Recognition of alluvial fan deposits in the stratigraphic record, in J.K. Rigby and W.K. Hamblin, eds., Recognition of ancient sedimentary environments: SEPM Special Pub. 16, p. 63-83.
- Chamberlain, C.K., 1978, Recognition of trace fossils in cores, in P.B. Basan, ed., Trace fossil concepts: SEPM Short Course 5, p. 119-179.
- Committee of Panhandle Geological Soc., 1955, Stratigraphic correlation chart of Texas Panhandle and surrounding region: Panhandle Geologic Soc., Box 2473, Amarillo, Texas.

- Dutton, S.P., 1980a, Depositional systems and hydrocarbon resource potential of the Pennsylvanian System, Palo Duro and Dalhart basins, Texas Panhandle: University of Texas at Austin, Bureau of Economic Geology Geological Circular 80-8, 49 p.
- _____, 1980b, Petroleum source rock potential and thermal maturity, Palo Duro Basin, Texas: University of Texas at Austin, Bureau of Economic Geology Geological Circular 80-10, 48 p.
- _____, 1982, Pennsylvanian fan-delta and carbonate deposition, Mobeetie field, Texas Panhandle: AAPG Bulletin, v. 66, p. 389-407.
- _____, R.J. Finley, W.E. Galloway, T.C. Gustavson, C.R. Handford, and M.W. Presley, 1979, Geology and geohydrology of the Palo Duro Basin, Texas Panhandle: University of Texas at Austin, Bureau of Economic Geology Geological Circular 79-1, 99 p.
- _____, A.G. Goldstein, and S.C. Ruppel, 1982, Petroleum potential of the Palo Duro Basin, Texas Panhandle: University of Texas at Austin, Bureau of Economic Geology Report of Investigations No. 123, 87 p.
- Eddleman, M.W., 1961, Tectonics and geologic history of the Texas and Oklahoma Panhandles, in Oil and Gas fields of the Texas and Oklahoma Panhandles: Panhandle Geol. Soc., p. 61-68.
- Evans, J.L., 1979, Major structural and stratigraphic features of the Anadarko basin, in N.J. Hyme, ed., Pennsylvanian sandstones of the mid-continent: Tulsa Geol. Soc., Tulsa, Oklahoma, p. 97-113.
- Friedman, G.M. and J.E. Sanders, 1978, Principles of sedimentology: New York, John Wiley and Sons, p. 303-305.
- Flawn, P.T., 1965, Basement-not the bottom of the beginning: AAPG Bulletin, v. 49, p. 883-886.
- Folk, R.L., 1980, Petrology of sedimentary rocks: Austin, Hemphill Publishing Co., p. 127.
- Fritz, M., 1986, DOE releasing Palo Duro study, in V. Stefanic, ed., AAPG Explorer, Tulsa, Oklahoma, March, p. 1, 20-21.
- Galloway, W.E., T.E. Ewing, C.M. Garrett, N. Tyler, and D.G. Bebout, 1983, Atlas of major Texas oil reservoirs, W.L. Fisher, Director: The University of Texas at Austin, Bureau of Economic Geology, Texas, 78712.
- Handford, C.R., and S.P. Dutton, 1980, Pennsylvanian-Lower Permian depositional systems and shelf margin evolution, Palo Duro Basin, Texas: AAPG Bulletin, v. 64, p. 88-106.

- Hjulstrom, Filip, 1935, Studies of morphological activity of rivers as illustrated by the River Fyris: Upsala Univ. Mineralogisk-Geologiska Institute Bulletin, v. 25, p. 221-527.
- Klein, G., 1982, Sandstone depositional models for exploration for fossil fuels: Boston, International Human Resources Development Corporation, p. 8-20.
- Kluth, C.F., and P.J. Coney, 1981, Plate tectonics of the Ancestral Rocky Mountains: Geology, v. 9, p. 10-15.
- Locke, K.A., 1983, Trace fossil assemblages in selected shelf sandstones: Master's thesis, Texas A&M University, College Station, Texas, 136 p.
- McCasland, R.D., 1980, Subsurface geology of the Dalhart Basin, Texas Panhandle: Master's thesis, Texas Tech University, Lubbock, Texas, 147 p.
- McGowen, J.H., 1970, Gum Hollow fan delta, Nueces Bay, Texas: University of Texas at Austin, Bureau of Economic Geology Report of Investigations No. 69, 91 p.
- Meyer, R.F., 1966, Geology of Pennsylvanian and Wolfcampian rocks in Southeast New Mexico: New Mexico Bureau of Mines and Mineral Resources, Mem. 17, 123 p.
- Muehlberger, W.R., R.E. Denison, and E.G. Lidiak, 1967, Basement rocks in continental interior of United States: AAPG Bulletin, v. 51, p. 2351-2380.
- Nicholson, J.H., 1960, Geology of the Texas Panhandle, in Aspects of the geology of Texas, a symposium: University of Texas at Austin, Bureau of Economic Geology Publication 6017, p. 51-64.
- Neilson, T.H., 1982, Alluvial fan deposits, in P.A. Scholle and D. Spearing, eds., Sandstone depositional environments: AAPG Memoir 31, p. 49-86.
- Pickett, G.R., 1966, A review of current techniques for determination of water saturation from logs: Journal of Petroleum Technology, v. 17, p. 1425-1433.
- Pippin, L., 1970, Panhandle-Hugoton Field, Texas, Oklahoma, and Kansas, The first fifty years: AAPG Memoir 14, p. 204-222.
- Rogatz, H., 1935, Geology of the Texas Panhandle oil and gas field: AAPG Bulletin, v. 19, p. 1089-1109.

- Roth, R., 1949, Paleogeology of the Panhandle of Texas: Geol. Soc. America Bulletin, v. 60, p. 1671-1688.
- Schopf, J.M., 1975, Pennsylvanian climate in the United States, in McKee, E.D., and Crosby, E.J., coord., Paleotectonic Investigations of the Pennsylvanian System, Part II: Interpretive Summary and Special Features of the Pennsylvanian System: U.S. Geol. Survey Prof. Paper 853, p. 23-31.
- Tissot, B.P. and D.H. Welte, 1978, Petroleum formation and occurrence: New York, Springer-Verlag, 539 p.
- Waples, D.W., 1980, Time and temperature in petroleum exploration: Application of Lopatin's method to petroleum exploration: AAPG Bulletin, v. 64, p. 916-926.
- Wescott, W.A., and F.G. Ethridge, 1980, Fan-delta sedimentology and tectonic setting-Yallahs fan delta, Southeast Jamaica: AAPG Bulletin, v. 64, p. 374-399.

APPENDICES

The following pages include:

- I) Well symbol identification.
- II) Index map of study area showing well control and locations of cross sections.
- III) Petrographic analysis and core descriptions of:
 - A) Jay Taylor B-1 (L-2)
 - B) Parker Creek 1 (S27)
- IV) Rock fragment/feldspar ratio vs. grain size data.
- V) Structure map data.
- VI) Isopach map data.
- VII) Jay Taylor B-1 (L-2) core analysis.

APPENDIX I

WELL SYMBOL IDENTIFICATION

Symbol	Well Name	Field	League/Section	Spud Date (month-year)	Depth	Elev. (K. B.)	Type (month-year)
L1	Jay Taylor A-1	Lambert 1	S82	12-78	7500	3617	011
L2	Jay Taylor B-1	Lambert 1	S82	1-79	7425	3610	011
L3	Jay Taylor D-1	Lambert 1	S82	5-79	7550	3652	011
L4	Fulton-King A-1	Lambert 1	S82	2-79	7227	3600	011
L5	Fulton-King A-2	Lambert 1	S82	3-79	7204	3577	011
L6	Fulton-King A-3	Lambert 1	L317	4-79	7300	3608	011
L7	Fulton-King A-4	Lambert 1	S82	6-79	7275	3594	SMD
L8	Fulton-King A-5	Lambert 1	L317	2-80	7531	3665	Dry
L9	Fulton-King A-6	Lambert 1	S82	4-81	7433	3540	Shut in (12-81)
L10	Fulton-King A-7	Lambert 1	L317	9-82	7400	3669	Dry
L11	Fulton Ranch 1	Lambert 1	L317	7-85	7270	3617	Dry
H12	Aurora 1	Hryhor	L316	2-82	7822	3584	011
H13	Aurora 2	Hryhor	L316	2-82	7722	3590	011
H14	Aurora 3	Hryhor	L316	3-82	7800	3567	011
H15	Aurora 4	Hryhor	L316	3-82	7500	3555	011
H16	Aurora 5	Hryhor	L317	3-82	8024	3563	Dry
H17	Aurora 6	Hryhor	L316	4-82	7815	3575	011
H18	Aurora 7	Hryhor	L317	4-82	7511	3551	011
H19	Aurora 8	Hryhor	L316	5-82	7504	3613	011
H20	Aurora 9	Hryhor	L316	5-82	7700	3575	011
H21	Aurora 10	Hryhor	L316	5-82	7500	3563	011
H22	Aurora 11	Hryhor	L317	5-82	7323	3538	011
H23	Aurora 12	Hryhor	L316	5-82	7900	3593	Dry
H24	Aurora 13	Hryhor	L316	7-82	7511	3568	011

Appendix I (continued)

Symbol	Well Name	Field	League/Section	Spud Date (month-year)	Depth	Elev. (K.B.)	Type (month-year)
H25	Aurora 14	Hryhor	L316	6-82	7575	3539	SMD
H26	Aurora 15	Hryhor	L316	9-82	7500	3580	011
S27	Parker Creek 1	Sundance	L316	7-81	7608	3603	Shut-In (1-86)
S28	Parker Creek 2	Sundance	L316	8-81	7600	3613	011
S29	Parker Creek 3	Sundance	L307	10-81	7518	3570	011
S30	Parker Creek 4	Sundance	L316	11-81	7610	3635	011
S31	Parker Creek 5	Sundance	L307	12-81	7500	3575	Dry
S32	Parker Creek 6	Sundance	L316	12-81	7650	3670	011
S33	Parker Creek 7	Sundance	L316	12-81	7600	3580	Shut In (7-85)
S34	Parker Creek 8	Sundance	L316	1-82	7650	3640	011
S35	Parker Creek 9	Sundance	L307	2-82	7700	3574	Dry
S36	Parker Creek 10	Sundance	L316	2-82	7650	3677	Shut-In (10-84)
S37	Parker Creek 11	Sundance	L316	3-82	7616	3669	Shut in (7-83)
S38	Parker Creek 12	Sundance	L316	7-82	7500	3690	011
S39	Parker Creek 13	Sundance	L316	8-82	7500	3684	011
S40	Parker Creek 14	Sundance	L316	8-82	7510	3693	Shut-In (7-84)
S41	Parker Creek 15	Sundance	L316	8-82	7500	3585	011
N42	Neptune 1	Neptune	L316	5-82	7860	3658	011
N43	Neptune 2	Neptune	L316	5-82	7800	3643	Dry
N44	Neptune 3	Neptune	L316	5-82	7620	3692	Shut-In (7-85)
P45	Amy 1	Peripheral	S85	12-82	7248	3683	011

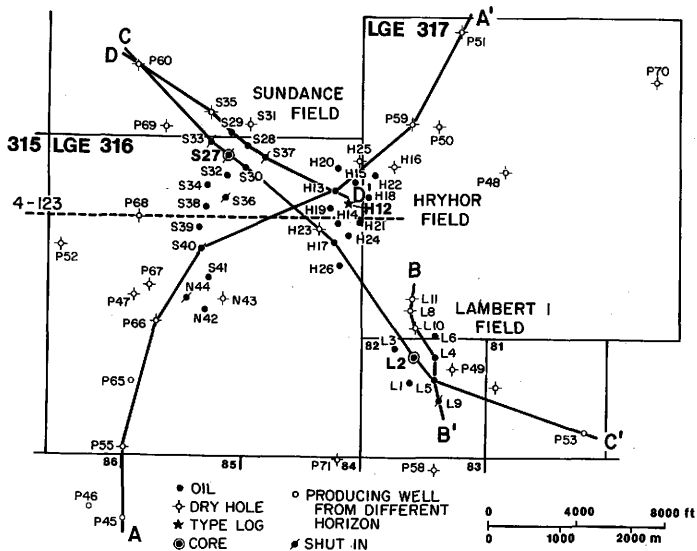
Appendix I (continued)

Symbol	Well Name	Field	League/Section	Spud Date (month-year)	Depth	Elev. (K.B.)	Type (month-year)
P46	Amy 2	Peripheral	S86	3-83	7015	3745	Shut-In (5-84)
P47	Connie 1	Peripheral	L316	3-83	7800	3726	Dry
P48	Cottonwood Camp 1	Peripheral	L317	9-81	7920	3570	Dry
P49	Diana 1	Peripheral	S81	9-82	7300	3550	Dry
P50	Exotic 1	Peripheral	L317	12-79	8300	3550	Dry
P51	Fulton Iris 1	Peripheral	L317	4-82	8257	3568	Dry
P52	Gravel Pit 1	Peripheral	L316	10-79	7630	3744	Dry
P53	Hebe 1	Peripheral	S81	8-82	7364	3521	Gas
P55	Jay Taylor E-1	Peripheral	L316	4-80	7530	3750	Dry
P58	Mitchell Creek 1	Peripheral	S83	11-81	7200	3570	Dry
P59	New Atlantis 1	Peripheral	L317	9-82	8000	3625	Dry
P60	Parker Camp 1	Peripheral	L307	10-82	7970	3572	Dry
P65	Sharan 1	Peripheral	L316	9-83	7450	3717	Oil
P66	Singlefold 1	Peripheral	L316	1-81	7790	3707	Dry
P67	South Parker Creek 1	Peripheral	L316	7-82	7800	3725	Dry
P68	Spring Creek 1	Peripheral	L316	10-82	7600	3596	Dry
P69	Sunshine 1	Peripheral	L307	10-79	7757	3620	SMD
P70	Ware Jupiter 1	Peripheral	L317	4-82	8150	3613	Dry
P71	York 1	Peripheral	S84	12-83	7647	3585	Dry

Note: Kelly Bushing (K.B.) -10 = Ground Level

SMD = Salt Water Disposal

APPENDIX II



APPENDIX III

PETROGRAPHIC ANALYSES AND CORE DESCRIPTIONS

- Appendix III-A Jay Taylor B-1 (L2)
 Lambert 1 Field
 Oldham, County, Texas
- Appendix III-B Parker Creek 1 (S27)
 Sundance Field
 Oldham, County, Texas

Core descriptions and petrographic analyses abbreviations include:

ft = feet
in = inches
mm = millimeter

Petrographic analyses table superscript notations include:

Grain size^a - Long axis measurements; Max = Maximum Size,
 σ = standard deviation

Detrital Composition^b; Qz = monocrystalline quartz, F = feldspar,
Rx = rock fragments including polycrystalline quartz, Oth
= other detrital grains, Mx = matrix (clays and chlorite).

Cement^c; CO₃ = carbonate cement.

PETROGRAPHIC ANALYSIS

Jay Taylor B-1 (L2)

Lambert 1 Field

Oldham County, Texas

Core: 6751-6802 and 6809.5-6862.5

Depth (ft)	Grain Size ^a			Detrital Composition ^b								Cement ^c		Porosity % of total
	Mean mm	Max mm	σ mm	Gravel (> 2 mm)				Sand (< 2 mm)				Mx %	CO ₃ % of total	
				Qz %	F %	Rx %	Oth %	Qz %	F %	Rx %	Oth %			
6751	1.1	4.6	1.3	7	10	30	0	10	32	7	<1	4	8	15
6755	2.5	5.6	1.4	6	20	26	0	8	26	6	<1	8	11	13
6756	1.4	6.8	1.8	3	3	14	0	20	33	15	<1	12	0	15
6757	1.5	5.7	1.3	0	4	16	0	21	33	21	<1	5	0	13
6773	1.6	4.8	1.2	4	12	13	0	11	38	15	1	6	9	8
6781	1.6	7.2	1.8	0	1	14	0	22	48	7	1	7	1	5
6784	1.2	5.8	1.3	3	5	10	0	27	31	18	3	3	2	11
6787	1.4	6.0	1.3	3	4	19	0	17	32	15	2	8	2	10
6796	0.36	3.2	0.66	0	1	1	0	20	21	6	3	48	0	0
6798	1.5	7.3	1.5	2	6	10	0	30	35	13	1	3	14	3
6812.5	1.5	4.5	1.3	3	2	16	0	18	41	15	2	3	0	8
6813	2.4	12.4	1.9	1	20	21	0	8	29	6	2	13	3	4
6815	0.73	3.1	0.65	0	1	3	0	22	57	13	3	1	0	9
6823	1.2	5.4	1.3	0	5	7	0	22	43	15	8	0	6	10
6826	2.6	9.6	2.0	8	21	21	0	15	26	5	2	2	15	5
6833.2	0.83	3.9	0.77	1	3	4	0	18	67	5	<1	2	0	11
6839	1.7	8.1	2.5	3	11	9	0	28	40	3	<1	6	3	4
6845.5	1.5	6.1	1.7	5	7	10	0	15	44	6	5	8	0	7
6852	0.52	2.4	0.44	0	0	0	0	26	53	9	4	8	0	10
6861	2.2	7.7	1.7	9	17	23	0	12	26	8	<1	5	2	16

^aLong-axis measurements; σ = standard deviation.

^bQz = monocrystalline quartz, F = feldspar, Rx = rock fragments including polycrystalline quartz,

Oth = other detrital grains, Mx = matrix (clays and chlorite).

^cCO₃ = carbonate cement.

CORE DESCRIPTION

Jay Taylor 8-1 (L2)

Lambert 1 Field

Oldham County, Texas

Canyon Granite Wash Conglomerate

Core: 6750.8-6802.1 and 6809.5-6862 feet (6752.8-6804.1 and 6811.5-6864 feet corrected to electric log).

Depth (ft)	Thickness (ft)	Description
6750.8	.2	Shale; black; very silty; thin, even, parallel, horizontal, continuous laminae; finely bioturbated with 2 mm gray lenses; apparent high organic content; sharp basal contact.
6751	14.3	Conglomerate and sandstone; gray; fine sand- to pebble-grained; poorly-sorted, pebbles are subangular to subrounded, granitic, even, parallel, continuous laminae inclined 18-21°; patchy cement; abundant charcoal flakes; maximum pebble size is 18 mm. Interbedded with .5-1 mm shale laminae at 6756.7. Wavy, irregular, .5-1 mm shale lamina basal contact. Thin section: 6751 6755 6756 6757
6765.3	4.5	Conglomerate and sandstone; reddish gray; very-coarse sand to pebble-grained; poorly sorted; pebbles are subangular to subrounded, granitic, even, parallel, continuous laminae inclined 18-20°; moderately cemented; abundant charcoal flakes; maximum pebble size is 22 mm; wavy, irregular basal contact.
6769.8	4.2	Conglomerate and sandstone; pinkish gray; fine-sand to pebble-grained; poorly sorted, pebbles are subangular to subrounded, granitic; even, parallel, continuous laminae inclined 16°; maximum pebble size is 10 mm. Thin section: 6773
6774	3.0	Core missing.
6777	11.0	Conglomerate and sandstone; gray; fine-sand to pebble-grained; poorly sorted; pebbles are subangular to subrounded, granitic; 10-30 cm fining upward sets; even, parallel, horizontal, continuous laminae; maximum pebble size is 13 mm. Wavy, irregular, .5 mm shale lamina at 6781.5. Wavy, irregular, basal contact. Thin section: 6781 6784 6787

Jay Taylor B-1 (L2) (continued)

Depth (ft)	Thickness (ft)	Description
6788	6.0	Conglomerate and sandstone; gray; fine- to pebble-grained; poorly sorted; pebbles are subround to subangular, granitic; even, parallel, continuous laminae inclined 14°; moderately cemented; maximum pebble size is 11 mm, .5-1 mm shale lamina basal contact.
6794	1.0	Conglomerate and sandstone; reddish gray; medium-sand to granule-grained; moderately sorted; granules are angular to subrounded, granitic; well cemented; wavy dolomite veins 2-3 mm thick; maximum granule size is 4 mm. Sharp basal contact.
6795	1.0	Shale; black; very silty; .5-1 mm, even, parallel, horizontal, continuous laminae; broken and fragmented crinoid stems increase in abundance downward; finely bioturbated with 2-3 mm gray lenses; gradational contact.
6796	.9	Silty mudstone; brown; suspended medium sand- to granule-size grains; scattered broken and fragmented crinoid stems. Thin section: 6796
6796.9	1.6	Conglomerate and sandstone; pinkish gray; fine-sand to pebble-grained; poorly sorted; pebbles are subangular to subrounded, granitic; even, parallel, continuous laminae inclined 19°; well cemented; maximum pebble size is 8 mm. Gradational contact. Thin section: 6798
6798.5	3.6	Conglomerate and sandstone; pinkish gray; very-fine sand- to pebble-grained; poorly sorted; pebbles are subangular to subrounded, granitic; even, parallel, continuous laminae inclined 6°; 7-15 cm fining upward sets; .5-2 mm charcoal flakes increase in abundance downward; maximum pebble size is 18 mm.
6802.1	6.9	Core missing.
6809	3.5	Conglomerate and sandstone; pinkish gray; fine sand- to pebble-grained; poorly sorted; pebbles are angular to rounded, granitic; abundant black shale flakes; even, parallel, continuous laminae inclined 21°; maximum pebble size is 12 mm; wavy, irregular, .5-1 mm shale lamina basal contact.
6812.5	1.0	Conglomerate and sandstone; reddish gray; fine sand- to pebble-grained; poorly sorted; pebbles are angular to subrounded, granitic; black, wavy, .5-2 mm thick and 25 mm long discontinuous shale clasts; irregular, .5 mm shale lamina basal contact. Thin section: 6812.5 6813

Jay Taylor B-1 (L2) (continued)

Depth (ft)	Thickness (ft)	Description
6813.5	3.0	<p>Conglomerate and sandstone; gray; very-fine sand- to pebble-grained; very poorly sorted; pebbles are subangular to rounded, granitic; even, parallel, continuous laminae inclined 21°; black, .5 mm, wavy shale laminae at 6814; maximum pebble size is 16 mm; irregular, .5 mm shale lamina basal contact.</p> <p>Thin section: 6816.5</p>
6816.5	5.7	<p>Conglomerate and sandstone; orangish gray; fine sand- to pebble-grained; very poorly sorted; pebbles are angular, granitic; even, parallel, continuous laminae inclined 5-6 °; black, wavy, 2 mm wide and 16 mm long shale clasts at 6821.6; abundant black crystalline charcoal flakes; maximum pebble size is 9 mm; wavy, irregular, .5 mm shale lamina basal contact.</p>
6822.2	10.8	<p>Conglomerate and sandstone; gray; fine sand- to pebble-grained; poorly sorted; pebbles are angular to subrounded, granitic; even, parallel, continuous laminae inclined 16°; 2.3-4.2 cm fining upward sets; abundant .5-3 mm long and .5 mm thick black charcoal flakes; maximum pebble size is 19 mm; .5 shale lamina at 6829.3, 6822.4, and 6833. Wavy, irregular, 2 mm black shale lamina basal contact.</p> <p>Thin section: 6823 6826</p>
6833	6.4	<p>Conglomerate and sandstone; gray; fine sand- to pebble-grained; poorly sorted; pebbles are angular to subangular, granitic; even, parallel, continuous laminae inclined 15°; even, parallel, horizontal, continuous laminae at 5833-5834.3, and 6835.2-6836.4; abundant black charcoal flakes; black shale lamina at 6835.2, 6837.3, 6837.6, 6838, 6838.8, and 6839; maximum pebble size is 8 mm. At 6838.2-6839 fine to medium grained, no pebbles. Irregular, .5-1 mm shale lamina basal contact.</p> <p>Thin section: 6833.2 6839</p>
6839.4	12.6	<p>Conglomerate and sandstone; gray; fine sand- to pebble-grained; poorly sorted; pebbles are subangular to rounded, granitic; even, parallel, horizontal, continuous laminae to even, parallel, continuous laminae inclined 9°; 21 mm long and 1 mm thick charcoal clasts; shale lamina at 6845.2, 6846, 6848.1, 6849, 6849.5; sharp coarse grain basal contact.</p> <p>Thin section: 6845.5</p>

Jay Taylor B-1 (L2) (continued)

Depth (ft)	Thickness (ft)	Description
6852	10.0	Conglomerate and sandstone; gray; fine- to pebble-grained; poorly sorted; pebbles are subround to rounded; even, parallel, discontinuous laminae inclined 3°; discontinuous shale laminae at top; coarsening downward to 6852.8; 6852.8-6862 has 25-60 cm fining upward sets, maximum pebble size is 9 mm. Generally finer grained than above section. Thin section: 6852 6861

PETROGRAPHIC ANALYSIS
 Parker Creek 1 (S27)
 Sundance Field
 Oldham County, Texas
 Core: 7032-7050 and 7064-7088

Depth (ft)	Grain Size ^a			Detrital Composition ^b								Cement ^c		Porosity % of total
	Mean	Max	σ	Gravel (> 2 mm)				Sand (< 2 mm)				Mx	CO ₃	
	mm	mm	mm	Qz %	F %	Rx %	Oth %	Qz %	F %	Rx %	Oth %	% of total	% of total	
7032	2.1	8.0	1.9	3	6	19	0	24	31	14	<1	3	14	3
7038	0.26	1.3	0.17	0	0	0	0	23	54	8	6	9	1	6
7042	1.2	8.8	1.4	3	1	9	0	31	44	7	1	4	0	1
7043	0.84	4.8	0.95	2	4	6	0	11	55	19	<1	3	0	12
7045	0.11	0.32	0.07	0	0	0	0	38	28	0	3	31	0	0
7046	0.23	0.79	0.14	0	0	0	0	27	55	4	2	12	0	2
7065.5	2.3	6.4	1.4	3	8	33	0	2	43	10	<1	1	7	0
7068	0.18	2.5	0.31	1	0	0	0	26	39	2	3	29	0	0
7073	0.39	3.4	0.53	0	0	1	0	24	46	6	<1	23	0	0
7074	0.13	0.44	0.09	0	0	0	0	36	36	1	2	25	1	0
7083	2.0	9.5	2.3	1	7	21	0	29	28	12	1	1	16	2
7084	1.0	8.2	1.3	1	8	0	0	29	52	6	3	1	12	2
7085	0.12	0.24	0.05	0	0	0	0	26	42	3	6	23	1	3

^aLong-axis measurements; σ = standard deviation.

^bQz = monocrystalline quartz, F = feldspar, Rx = rock fragments including polycrystalline quartz;
 Oth = other detrital grains, Mx = matrix (clays and chlorite).

^cCO₃ = carbonate cement.

CORE DESCRIPTION

Parker Creek 1 (S27)

Sundance Field

Oldham County, Texas

Canyon Granite Wash Conglomerate

Core: 7032.3-7050 and 7074-7088 feet (7933.8-7051.5 and 7065.5-7089.5 feet corrected to electric log).

Depth (ft)	Thickness (ft)	Description
7032.3	4.2	Conglomerate and sandstone; reddish gray; medium sand- to pebble-grained; pebbles are angular to subrounded; even, parallel, horizontal, continuous laminae at the top, grades downward to even, parallel, continuous laminae inclined 18-20°; 6-12 cm fining upward sets; maximum pebble size is 56 mm; no shale lamina; sharp, wavy basal contact. Thin section: 7032
7036.5	4.5	Silty mudstone; black to dark gray; uneven, nonparallel, discontinuous, wavy, truncated laminae; 4 mm shale clast at 7038; very fine grained sand increases downward to 7039, then decreases to black siltstone at base. Gradational contact, abundant soft sediment deformation; pyrite nodules at 7040.1. Thin section: 7038
7041	2.0	Silty mudstone; black to gray; uneven, nonparallel, discontinuous, wavy laminae; matrix supported pebbles and medium grained sand increase downward to gradationally become a fine sand to pebble grained, well cemented conglomerate. Sharp basal contact. Thin section: 7042
7043	.5	Silty mudstone; black; 15 mm mass composed of medium sand- to granule- sized grains suspended in silt; coarsens downward to medium grained sandstone; sharp basal contact. Thin section: 7043
7043.5	1.0	Sandstone; light tan; very-fine grained; uneven, nonparallel, discontinuous laminae; 5-10 cm fining upward sets. Sharp basal contact.
7044.5	5.5	Silty mudstone; black to dark gray; interbedded with very fine to coarse grained sand; uneven, nonparallel, wavy, discontinuous, truncated sand lenses; abundant soft sediment deformation; granule size grains are matrix supported at 7048-7049.8. Thin section: 7045 7046
7050	13.8	Core missing.

Parker Creek 1 (S27) (continued)

Depth (ft)	Thickness (ft)	Description
7063.8	.2	Silty mudstone; black; even, parallel, slightly wavy, continuous laminae overlies fine to coarse grained sand, separated by a sharp contact.
7064	1.5	Shale; black; very silty; .5-1 mm, even, parallel, horizontal continuous laminae; finely bioturbated with 2 mm gray lenses; sharp basal contact.
7065.5	.5	Conglomerate and sandstone; gray; fine sand to granule grained; poorly sorted, granules are subangular to subrounded, granitic; massive; sharp basal contact. Thin section: 7065.5
7066	7.0	Silty mudstone; gray to black; uneven, parallel, wavy, horizontal, continuous laminae; fine to medium grained sand increases downward from 7065-7067, 7071-7071.8, 7072.8-7073 (all fining upward sets); sharp, wavy basal contact. Thin section: 7068
7073	3.1	Silty mudstone; gray to black; occasionally sandy; even, parallel, wavy, continuous laminae; fine to pebble grained sand increases downward from 7073.4-7073.8; 4 mm wide and 11 mm long pebble lenses at 7074.5; coarsening upward set at 7075.6 with 20 mm shale clast; sharp, wavy basal contact. Thin section: 7073 7074
7076.1	10.9	Silty mudstone; gray to black; occasionally sandy; uneven, parallel, wavy, continuous laminae; coarsely bioturbated; fine to pebble grained sand interbedded at 7076.2-7076.3, 7079.4-7079.5, 7079.9-7080.2, 7080.5-7080.8, 7081.8-7081.9, 7083, 7084.8 (all fining upward sets); sharp basal contact. Thin section: 7083 7084 7085
7087	1.0	Shale; very black; uneven, parallel, wavy to horizontal, continuous, laminae; apparent high organic content.

APPENDIX IV

ROCK FRAGMENT/FELDSPAR RATIO VS. GRAIN SIZE DATA

Well Symbol	Mean Grain Size	Rock Fragment Rx %	Feldspar F(%)	Rx/F Ratio
L2	1.1	37	42	0.88
	2.5	32	46	0.69
	1.4	29	36	0.81
	1.5	37	37	1.00
	1.6	28	50	0.56
	1.6	21	49	0.43
	1.2	28	36	0.78
	1.4	34	36	0.94
	0.36	7	22	0.32
	1.5	23	41	0.56
	1.5	31	43	0.72
	2.4	27	49	0.55
	0.73	26	58	0.44
	1.2	22	48	0.46
	3.6	26	47	0.55
	0.83	9	70	0.13
	1.7	12	51	0.24
	1.5	16	51	0.31
	0.52	9	53	0.17
	2.2	31	43	0.72
S27	2.1	33	37	0.89
	0.26	8	54	0.15
	1.2	16	45	0.35
	0.84	25	59	0.42
	0.11	0	28	0.0
	0.23	4	55	0.07
	2.3	43	51	0.84
	0.18	2	39	0.05
	0.39	7	46	0.15
	0.13	1	36	0.03
	2.0	33	35	0.94
	1.0	6	60	0.10
	0.12	3	42	0.07

Equation of the least squares regression line is $\log y = m \log x + \log b$

The equivalent equation of the line is $y = bx^m$

Values are: $b = .35$

$m = .90$

Correlation coefficient is 0.84.

APPENDIX V

STRUCTURE MAP DATA

The following abbreviations apply to the column headings:

Cim - Cimmaron
Tubb - Tubb
Red Ca - Red Cave
Pan Lm - Panhandle Lime
Brn Dolo - Brown Dolomite
Cis Sh - Cisco Shale
Man GW - Manarte Granite Wash
Can Lm - Canyon Limestone
Can GW - Canyon Granite Wash
Stra Lm - Strawn Limestone
Stra GW - Strawn Granite Wash
PC - Precambrian Granite

The following abbreviations apply to the well symbol:

L - Lambert I Field
H - Hryhor Field
S - Sundance Field
N - Neptune wells
P - Peripheral wells

The following abbreviations apply to missing data in the columns:

NA - Not Available
NP - Not Present
NDE - Not Deep Enough

Structure Map Data

Symbol	Well Name	Elev.	Cfm	Tubb	Red Ca	Pan Ln	Brn Dolo	Cis Sh	Man GW	Can Ln	Can GW	Stra Ln	Stra GW	PC
L1	Jay Taylor A-1	3617	762	607	272	-286	-723	-2683	NP	-3123	-3151	-3529	-3588	-3791
L2	Jay Taylor B-1	3601	860	618	280	-274	-704	-2630	NP	-3052	-3078	-3420	-3452	-3599
L3	Jay Taylor D-1	3652	NA	NA	NA	-298	-742	-2728	NP	-3150	-3174	-3527	-3560	-3776
L4	Fulton-King A-1	3600	918	655	306	-262	-674	-2650	NP	NP	-3054	-3290	-3309	-3370
L5	Fulton-King A-2	3577	897	632	293	-281	-691	-2583	NP	-3061	-3067	-3415	-3448	-3583
L6	Fulton-King A-3	3608	NA	NA	NA	-274	-706	-2732	NP	NP	-3150	-3464	-3490	-3547
L7	Fulton-King A-4	3594	1049	644	309	-271	-678	-2780	NP	NP	-3200	-3515	-3540	-3586
L8	Fulton-King A-5	3665	885	605	261	-333	-770	-2860	NP	-3170	-3191	-3515	-3547	-3655
L9	Fulton-King A-6	3540	855	575	230	-345	-755	-2682	NP	-3245	-3252	-3625	-3680	-3782
L10	Fulton-King A-7	3669	919	630	290	-296	-713	-2686	NP	-3071	-3109	-3481	-3509	-3621
L11	Fulton Ranch 1	3617	899	635	274	-297	-735	-2815	NP	-3215	-3237	-3488	-3505	-3553
H12	Aurora 1	3584	894	595	269	-408	-816	-3106	NP	-3436	-3482	-3862	-3891	-4131
H13	Aurora 2	3590	888	590	260	-365	-819	-3045	NP	-3480	-3500	-3880	-3925	-4070
H14	Aurora 3	3567	875	563	247	-374	-833	-3007	NP	-3487	-3508	-3887	-3929	-4162
H15	Aurora 4	3555	905	615	255	-343	-777	-3129	NP	-3487	-3497	-3887	NDE	NDE
H16	Aurora 5	3563	929	615	258	-343	-782	-3167	NP	-3598	-3606	-3979	-4029	-4179
H17	Aurora 6	3575	875	557	230	-380	-834	-3135	NP	-3523	-3550	-3883	-3944	-4205
H18	Aurora 7	3551	901	601	241	-357	-816	-3149	NP	-3522	-3533	-3813	-3837	NDE
H19	Aurora 8	3613	891	585	253	-361	-819	-3127	NP	-3485	-3503	NDE?	NDE	NDE
H20	Aurora 9	3575	915	613	247	-347	-785	-3160	NP	-3570	-3578	-3847	-3869	-4047
H21	Aurora 10	3563	901	584	233	-362	-800	-3117	NP	-3489	-3515	-3925	NDE	NDE
H22	Aurora 11	3538	890	610	252	-346	-807	-3160	NP	NP	-3562	NDE	NDE	NDE
H23	Aurora 12	3603	893	563	251	-381	-839	-3097	NP	-3663	-3685	-4182	-4207	NDE
H24	Aurora 13	3568	879	568	246	-372	-832	-3115	NP	-3496	-3521	-3922	NDE	NDE
H25	Aurora 14	3539	939	624	269	-331	-770	-3161	NP	NP	-3624	-3861	-3891	-3991
H26	Aurora 15	3580	880	560	240	-382	-788	-3000	NP	-3508	-3534	NDE/NP	NDE/NP	NDE
S27	Parker Creek 1	3603	953	633	325	-287	-713	-3059	NP	-3372	-3407	-3767	-3845	-3897
S28	Parker Creek 2	3613	962	643	333	-285	-697	-3052	NP	-3385	-3405	-3763	-3821	-3857
S29	Parker Creek 3	3570	972	625	330	-285	-705	-3085	NP	-3402	-3430	-3730	-3805	-3870
S30	Parker Creek 4	3635	950	630	325	-281	-697	-3010	-3375	-3385	-3404	-3779	-3843	NDE

Structure Map Data (continued)

Symbol	Well Name	Elev.	Cfm	Tubb	Red Ca	Pan Ln	Brn DoLo	Cis Sh	Man GW	Can Ln	Can GW	Stra Ln	Stra GW	PC
S31	Parker Creek 5	3573	953	633	325	-290	-715	-3058	NP	-3469	-3476	-3765	NP	-3832
S32	Parker Creek 6	3670	962	630	330	-285	-692	-3010	NP	-3370	-3390	-3760	-3840	NDE
S33	Parker Creek 7	3580	958	630	329	-271	-675	-3080	NP	-3419	-3446	-3804	-3875	NDE
S34	Parker Creek 8	3640	926	608	300	-315	-695	-3035	NP	-3402	-3438	-3805	NP	NDE
S35	Parker Creek 9	3574	944	622	314	-356	-746	-3141	NP	-3579	-3605	-3916	-3984	-4029
S36	Parker Creek 10	3677	929	617	307	-303	-715	-3033	-3401	-3421	-3445	-3833	-3903	NDE
S37	Parker Creek 11	3669	937	611	321	-289	-686	-3091	NP	-3423	-3439	-3841	-3904	NDE
S38	Parker Creek 12	3690	920	606	290	-292	-724	-2962	NP	-3388	-3413	-3760	NDE	NDE
S39	Parker Creek 13	3684	919	604	276	-321	-712	-3011	NP	-3361	-3406	-3756	NDE	NDE
S40	Parker Creek 14	3693	904	601	274	-369	-757	-2942	-3402	-3417	-3457	NDE	NDE	NDE
S41	Parker Creek 15	3685	915	587	275	-343	-726	-3043	NP	-3440	-3485	NDE	NDE	NDE
N42	Neptune 1	3658	918	594	276	-337	-724	-2973	NP	-3392	-3439	-3770	-3882	-4014
N43	Npetune 2	3643	903	587	273	-341	-729	-2982	NP	-3455	-3492	-3852	-3959	-4062
N44	Neptune 3	3692	920	697	282	-330	-726	-2936	NP	-3408	-3465	-3753	NDE	NDE
P45	Amy 1	3683	958	621	303	-277	-675	NP	NP	-2685	NP	?	NP	-3397
P46	Amy 2	3745	955	630	315	-265	-658	NP	NP	-2635	?	-3213	NDE	NDE
P47	Connie	3726	911	596	276	-336	-732	-2944	-3400	-3423	-3466	-3632	-3846	-3984
P48	Cottonwood Creek 1	3570	NA	NA	300	-285	-720	-3012	NP	NP	-3535	?	?	-4210
P49	Diana 1	3550	888	630	280	-292	-714	-2666	NP	NP	-3237	-3598?	NP	-3620
P50	Exotic 1	3602	NA	NA	NA	NA	NA	-3112	NP	-3644	-3664	-4146?	-4201?	-4519
P51	Fulton Iris 1	3568	953	616	289	-340	-827	-3292	NP	NP	-3902	-4335	-4412	-4596
P52	Gravel Pit 1	3744	924	619	301	-338	-756	-3026	NP	-3374	-3486	-3626	-3788	NDE
P53	Hebe 1	3521	871	619	261	-321	-729	-2679	NP	NP	-3249	-3571	-3595	-3754
P55	Jay Taylor E-1	3750	926	635	320	-278	-650	-2795	NP	-3000	-3147	-3208	NP	-3495
P58	Mitchell Creek 1	3570	932	622	290	-288	-835	-2594	NP	-3120	-3140	-3342?	?	NDE?
P59	New Atlantis 1	3625	941	630	275	-327	-780	-3120	NP	-3603	-3625	-4059?	-4095	-4355

Structure Map Data (continued)

Symbol	Well Name	Elev.	Cim	Tubb	Red Ca	Pan Lm	Brn Do10	C1s Sh	Man GW	Can Lm	Can GW	Stra Lm	Stra GW	PC
P60	Parker Camp 1	3572	944	617	313	-363	-773	-3233	-3723	-3808	-3848	-4048	-4209	-4240
P65	Sharan 1	3717	NA	NA	313	-335	-679	-2793	NP	-3183	-3248	-3383	?	-3583
P66	Singlefold 1	3707	867	597	252	-333	-752	-2943	NP	-3432	-3495	-3668	?	-3988
P67	South Parker Creek 1	3725	915	605	283	-363	-725	-2924	-3390	-3420	-3455	-3633	-3845	-3905
P68	Spring Creek 1	3596	846	526	211	-409	-809	-3073	-3556	-3599	-3657	?	NDE	NDE
P69	Sunshine 1	3620	946	600	310	-330	-755	-3080	-3485	-3510	-3550	-3875	-3960	NDE
P70	Ware Jupiter 1	3613	973	653	295	-329	-835	-3309	NP	-4085	-4117	-4252	-4337	-4432
P71	York 1	3585	882	572	216	-374	-760	-2905	NP	-3395	-3423	-3743	-3863	-3975

APPENDIX VI
ISOPACH MAP DATA

Symbol	Well Name	Thickness Canyon Limestone (ft)	Approximate Oil Zone Thickness (ft)	Gross Thickness Canyon Granite Wash (ft)	Shale 225 API cut-off (ft)	Net Thickness Canyon Granite Wash (ft)
L1	Jay Taylor A-1	28	46	378	55	323
L2	Jay Taylor B-1	26	85	342	18	324
L3	Jay Taylor D-1	24	50	312	63	249
L4	Fulton-King A-1	0	155	236	38	198
L5	Fulton-King A-2	6	135	348	56	292
L6	Fulton-King A-3	0	50	314	38	276
L7	Fulton-King A-4	0	Dry	315	85	230
L8	Fulton-King A-5	21	Dry	324	43	281
L9	Fulton-King A-6	7	Shut In	373	25	348
L10	Fulton-King A-7	38	Dry	362	62	300
L11	Fulton Ranch 1	22	Dry	251	65	186
H12	Aurora 1	46	54	380	78	302
H13	Aurora 2	18	28	380	68	312
H14	Aurora 3	21	20	379	74	305
H15	Aurora 4	10	72	390	64	326
H16	Aurora 5	7	Dry	373	78	295
H17	Aurora 6	27	28	333	168	165
H18	Aurora 7	11	42	280	52	228
H19	Aurora 8	18	41	>372	68	>304
H20	Aurora 9	10	4	269	56	213
H21	Aurora 10	30	58	412	102	310
H22	Aurora 11	0	11	>230	40	>190
H23	Aurora 12	22	Dry	497	66	431
H24	Aurora 13	34	30	>392	122	>270

Isopach Map Data (continued)

Symbol	Well Name	Thickness Canyon Limestone (ft)	Approximate Oil Zone Thickness (ft)	Gross Thickness Canyon Granite Wash (ft)	Shale 225 API cutt-off (ft)	Net Thickness Canyon Granite Wash (ft)
H25	Aurora 14	0	Dry	237	66	171
H26	Aurora 15	26	27	>284	70	>214
S27	Parker Creek 1	35	Shut In	360	64	296
S28	Parker Creek 2	20	16	358	67	291
S29	Parker Creek 3	28	26	300	46	254
S30	Parker Creek 4	18	16	375	50	325
S31	Parker Creek 5	7	Dry	288	28	260
S32	Parker Creek 6	20	52	370	46	324
S33	Parker Creek 7	27	Shut In	358	74	284
S34	Parker Creek 8	36	52	367	49	318
S35	Parker Creek 9	26	Dry	311	93	218
S36	Parker Creek 10	24	Shut In	388	68	320
S37	Parker Creek 11	16	Shut In	400	36	364
S38	Parker Creek 12	25	94	347	70	277
S39	Parker Creek 13	45	52	350	84	266
S40	Parker Creek 14	40	Shut In	>401	52	>349
S41	Parker Creek 15	45	8	>382	60	>322
N42	Neptune 1	47	27	331	66	265
N43	Neptune 2	37	Dry	360	106	254
N44	Neptune 3	57	Shut In	288	62	226
P45	Amy 1	712		0	0	0
P46	Amy 2	>572		0	0	0
P47	Connie 1	43	Dry	166	56	110
P48	Cottonwood Camp 1	0	Dry	364	40	324
P49	Diana 1	0	Dry	361	83	278

Isopach Map Data

Symbol	Well Name	Thickness Canyon Limestone (ft)	Approximate Oil Zone Thickness (ft)	Gross Thickness Canyon Granite Wash (ft)	Shale 225 API cutt-off (ft)	Net Thickness Canyon Granite Wash (ft)
P50	Exotic 1	21	Dry	482	30	452
P51	Fulton Iris 1	0	Dry	433	58	375
P52	Gravel Pit 1	112	Dry	140	12	128
P53	Hebe 1	0	Dry	322	56	266
P55	Jay Taylor E-1	157	Dry	51	4	47
P58	Mitchell Creek 1	20	Dry	202	13	189
P59	New Atlantis 1	22	Dry	434	58	376
P60	Parker Camp 1	40	Dry	200	62	138
P65	Sharan 1	65	Dry	135	40	95
P66	Singlefold 1	63	Dry	173	32	141
P67	South Parker Creek 1	44	Dry	178	40	138
P68	Spring Creek 1	58	Dry	>320	62	>258
P69	Sunshine	40	Dry	325	46	279
P70	Ware Jupiter 1	31	Dry	130	12	118
P71	York 1	28	Dry	320	163	157

APPENDIX VII

CORE ANALYSIS
Jay Taylor B-1 (L2)

Depth	Permeability (md)	Porosity (%)	Oil Saturation (%)	Water Saturation (%)
6751-52	170.0	11.2	5.7	60.1
6752-53	94.0	14.0	8.3	52.0
6753-54	613.0	16.1	11.3	55.1
6754-55	387.0	14.7	10.0	56.7
6755-56	145.0	13.5	9.9	55.4
6756-57	131.0	15.3	10.9	52.2
6757-58	76.0	14.2	6.6	51.2
6758-59	228.0	14.5	7.1	57.1
6759-60	82.0	8.2	9.2	59.8
6760-61	66.0	11.3	7.2	59.6
6761-62	37.0	15.1	8.0	55.3
6762-63	131.0	12.8	9.0	58.4
6763-64	80.0	14.4	9.1	53.6
6764-65	91.0	11.3	9.5	53.1
6765-66	18.0	11.2	9.0	59.3
6766-67	32.0	12.0	8.2	54.1
6767-68	24.0	13.0	8.0	54.6
6768-69	34.0	9.7	7.7	64.6
6769-70	4.6	8.8	5.5	67.1
6770-71	15.0	12.0	8.7	51.2
6771-72	37.0	13.1	8.3	59.8
6772-73	35.0	9.4	9.4	55.4
6773-74	21.0	13.8	8.8	60.7
6774-75	13.0	13.9	9.3	59.9
6775-76	26.0	8.2	8.2	55.4
6776-77	13.0	11.8	7.9	59.7
6777-78	22.0	13.1	8.7	57.3
6778-79	5.8	13.4	8.0	54.3
6779-80	8.2	12.5	7.9	52.0
6780-81	15.0	12.1	8.1	53.4
6781-82	6.3	11.4	7.6	59.8
6782-83	6.6	8.6	6.0	65.9
6783-84	40.0	13.4	7.0	55.0
6784-85	12.0	13.0	7.4	59.6
6785-86	65.0	14.1	9.5	50.1
6786-87	14.0	12.7	7.3	57.2
6787-88	24.0	12.0	7.0	55.3
6788-89	8.8	11.8	9.0	58.6
6789-90	12.0	11.6	7.5	58.0
6790-91	13.0	12.6	8.5	55.1
6791-92	0.4	3.5	3.9	71.3

Appendix 7 (continued)

Depth	Permeability (md)	Porosity (%)	Oil Saturation (%)	Water Saturation (%)
6792-93	0.2	4.1	4.5	70.9
6793-94	9.6	10.1	5.5	59.2
6794-95	0.1	1.7	2.1	77.7
6795-97	Shale			
6797-98	0.1	3.0	1.3	70.6
6798-99	1.6	9.0	3.2	66.9
6799-6800	22.0	11.5	6.5	58.7
6800-01	5.6	9.9	7.2	60.2
6801-02	112.0	15.7	9.6	53.5
6809-10	22.0	13.8	6.4	66.8
6810-11	23.0	15.2	5.5	62.5
6811-12	24.0	14.2	7.4	64.1
6812-13	1.0	12.5	7.8	69.6
6813-14	12.0	8.7	8.4	66.4
6814-15	4.4	6.8	6.2	67.2
6815-16	26.0	14.4	7.4	62.4
6816-17	24.0	15.6	7.1	67.8
6817-18	30.0	14.3	6.0	67.0
6818-19	17.0	12.6	6.0	62.4
6819-20	35.0	15.6	6.6	69.2
6820-21	53.0	14.2	8.1	62.8
6821-22	17.0	11.4	8.9	62.6
6822-23	290.0	12.1	8.9	66.0
6823-24	8.0	13.1	5.4	63.1
6824-25	28.0	14.4	6.1	60.2
6825-26	19.0	13.9	6.9	68.2
6826-27	9.7	8.9	8.7	58.1
6827-28	57.0	14.2	7.5	63.2
6828-29	38.0	11.7	6.6	57.6
6829-30	25.0	13.2	5.7	69.5
6830-31	19.0	16.0	5.8	67.7
6831-32	20.0	14.4	4.8	70.4
6832-33	18.0	14.3	4.3	70.1
6833-34	15.0	15.9	4.0	72.0
6834-35	6.8	14.7	5.5	76.4
6835-36	12.0	12.3	5.9	71.0
6836-37	13.0	14.3	7.2	65.1
6837-38	10.0	14.2	4.6	74.3
6838-39	5.4	4.0	2.1	83.5
6839-40	5.1	10.2	4.2	76.4
6840-41	12.0	15.5	4.4	75.5
6841-42	1.8	11.0	2.5	80.1
6842-43	22.0	14.6	2.8	71.3
6843-44	23.0	16.1	3.1	68.5

Appendix 7 (continued)

Depth	Permeability (md)	Porosity (%)	Oil Saturation (%)	Water Saturation (%)
6844-45	11.0	11.9	1.7	74.0
6845-46	6.1	12.0	2.1	76.6
6846-47	3.6	11.0	2.2	80.3
6847-48	5.7	11.8	0.0	83.7
6848-49	0.6	4.6	0.0	84.1
6849-50	6.5	12.0	0.0	85.0
6850-51	18.0	15.2	0.0	85.4
6851-52	7.7	13.3	0.0	87.5
6852-53	11.0	15.2	0.0	87.7
6853-54	13.0	15.7	0.0	88.2
6854-55	35.0	16.7	0.0	88.5
6855-56	19.0	16.0	0.0	90.7
6856-57	27.0	14.7	0.0	88.3
6857-58	64.0	15.2	0.0	88.2
6858-59	38.0	14.4	0.0	88.9
6859-60	53.0	15.1	0.0	86.3
6860-61	95.0	15.5	0.0	89.9
6861-62	123.0	14.7	0.0	86.9

Analysts by Core Laboratories, Inc.

VITA

NAME: Amy Laura Wharton
Mrs. James B. Vanderhill

BIRTHDATE: April 13, 1961

BIRTHPLACE: Galveston, Texas

PARENTS: Dr. and Mrs. James Taylor Wharton

EDUCATION: The University of Texas at Austin
Austin, Texas
B.S., 1983, Geological Sciences

**PROFESSIONAL
EXPERIENCE:** Baker and Taylor Drilling Co.
Amarillo, Texas
Summers: 1979, 1980, 1981, 1984

Tee Operating Co.
Lafayette, Louisiana
Summer: 1982

**PROFESSIONAL
MEMBERSHIPS:** American Association of Petroleum Geologists
Society of Professional Well Log Analyst

**PRESENT
EMPLOYMENT:** Mobil Oil Corporation
Dallas, Texas

**PERMANENT
ADDRESS:** c/o Dr. and Mrs. J.T. Wharton
10 Tokeneke Trail
Houston, Texas 77024

The typist for this thesis was Mrs. Myrna Armstrong